Faraday Discussions

Cite this: *Faraday Discuss.*, 2025, **259**, 200

ROYAL SOCIETY OF CHEMISTRY

PAPER

View Article Online
View Journal | View Issue

Open Access Article. Published on 14 januar 2025. Downloaded on 30-01-2026 17:48:09.
This article is licensed under a Creative Commons Attribution 3.0 Unported Licence.

The interplay of composition and mechanics in the thermodynamics of asymmetric ternary lipid membranes

Malavika Varma and Markus Deserno *

Received 9th December 2024, Accepted 13th January 2025
DOI: 10.1039/d4fd00196f

Eukaryotic lipid membranes are both compositionally complex and strongly asymmetric. Preferential lipid interactions enable coexistence between two fluid phases and an associated critical point, while bilayer asymmetry leads to leaflet-specific values for many observables—most saliently composition, but also a difference in leaflet tensions, for which we introduced the term "differential stress." Lipid mixing thermodynamics has been extensively studied, notably in idealized ternary model systems, and interest in asymmetry has grown significantly in the past decade, but their interplay remains poorly understood. Here we propose a conceptual framework for the thermodynamics of asymmetric ternary lipid membranes. Cholesterol emerges as an essential actor playing two different roles: first, it controls lipid mixing; second, it couples the compositional phase points of the two leaflets by achieving chemical equilibrium between them. Since differential stress can squeeze cholesterol from one leaflet into the other, this couples mechanical properties such as lateral stresses and curvature torques directly to mixing thermodynamics. Using coarse-grained simulations, we explore implications for leaflet coexistence, mechanical stability of giant vesicles, and differential stress driven phase segregation in a single leaflet. We hope this framework enables a fresh look at some persistent puzzles in this field, most notably the elusive nature of lipid rafts.

1 Introduction

Our overarching goal in this contribution is to develop a theoretical framework, largely based on thermodynamics, within which we can describe lipid membranes that are both compositionally complex and asymmetric. The scope for the composition degree of freedom will remain ostensibly modest: we do not aim to grapple with the enormous richness of biological lipid mixtures, and we will eschew proteins entirely. Instead, we will restrict our study to the widely studied case of ternary systems comprising a saturated lipid species, an unsaturated one, and cholesterol. These are the simplest known lipid mixtures that capture a phenomenon widely believed to be of physiological significance: the

Department of Physics, Carnegie Mellon University, Pittsburgh, PA 15213, USA

 This journal is © The Royal Society of Chemistry 2025

Open Access Article. Published on 14 januar 2025. Downloaded on 30-01-2026 17:48:09.
This article is licensed under a Creative Commons Attribution 3.0 Unported Licence.

possibility of coexistence between two fluid phases exhibiting different degrees of order. Considering bilayer asymmetry we will go beyond the usual discussion of leaflet-specific lipidomes and emphasize the importance of other thermodynamic variables that can differ between the two sides of the membrane, with an emphasis on stresses and torques.

This introduction serves to very briefly set the stage for these two main players—reminding our readers of a few key facts of complex biomembranes, and how these tend to be captured in simplified model systems.

1.1 Compositional complexity in nature

Biomembranes feature an astoundingly diverse lipidome:[1,2] thousands of chemically distinct lipids are synthesized in the endoplasmic reticulum (ER) of a typical eukaryotic cell, whose individual membrane organelles are kept at unique compositions while still hosting hundreds of individual species.[3] This complexity is challenging to even categorize,[4] but it is anything but random, even though its purpose is not well understood.

Since chemically distinct lipids interact differently with one another, we should expect that they do not mix ideally. If the interactions are sufficiently dissimilar, phase separation might occur. The by far most extensively studied instances of this possibility are "lipid rafts",[5–9] whose 2006 consensus definition describes them as "small (10–200 nm), heterogeneous, highly dynamic, sterol- and sphingolipid-enriched domains that compartmentalize cellular processes."[10] While having many putative effects on a wide spectrum of biomembrane functions, their precise nature (and even existence) has been famously controversial.[11,12] All the same, decades of data on highly non-ideal mixing need to be explained. Recent reviews[13,14] suggest that rafts will remain protagonists in this story, even though almost surely as more subtle actors than originally envisioned.

Of course, in addition to lipids, biomembranes also contain a host of peripheral or integral membrane proteins, which add further complexity, but for the sake of the present discussion we will summarily ignore them. This smacks of impermissible simplification, so let us offer a few thoughts to ease the discomfort:

(1) We will subsequently also ignore more than 99% of all lipid species, aiming for a model system that captures some emergent phase behavior, not an intricate lipidomic fingerprint.

(2) If the lipid matrix becomes laterally inhomogeneous, this will subsequently affect the proteins, but in a first step we can imagine them simply adjusting their distribution in response to the spatially nontrivial lipid background.

(3) In a second step, uneven protein partitioning between different lipid phases will in turn change the properties of these phases, further tweaking the distribution of lipids.

We can think of points 2 and 3 as the beginnings of an iterative process that adjusts the lipids, then the proteins, then again the lipids, then again the proteins—and so on. Mathematically, this constitutes a perturbation expansion in some lipid–protein coupling parameter. We will proceed on the hope that its first terms capture the main physics reasonably well. This is rigorously true if that coupling parameter is (in some sense) small—but, of course, this almost surely depends on the situation, and so we have to remain vigilant.

Open Access Article. Published on 14 januar 2025. Downloaded on 30-01-2026 17:48:09.
This article is licensed under a Creative Commons Attribution 3.0 Unported Licence.

1.2 Ternary model systems

Mixed membranes comprising hundreds of distinct lipid species cannot be studied with any expectation of experimental reproducibility and precise theoretical understanding. Model systems are clearly needed, but from the outset it is not obvious how far we may simplify. Remarkably, more than two decades of research strongly suggest that ternary systems consisting of a saturated lipid species, an unsaturated species, and cholesterol capture many of the key physical properties at the heart of biomembrane phase behavior.[15–31] Specifically, these systems exhibit the phenomenon of liquid–liquid phase separation, which offers tantalizing connections to raft-like domains. A particularly intriguing aspect is that the liquid–liquid coexistence region terminates in a critical point,[32–38] which has also been observed in cellular membranes (including its Ising-like critical exponents!).[39] This underscores the presence of universality—which often justifies the use of even highly simplified models.

1.2.1 Ternary phase diagrams. Phase diagrams of (symmetric) ternary lipid mixtures consisting of a saturated lipid, an unsaturated lipid, and cholesterol have been studied extensively. Since they will feature prominently in the rest of our discussion, we shall remind the reader of their main "topography", which will double as an opportunity to revisit the "Gibbs triangle" representation of ternary mixtures.

The constraint that the three mole fractions $\{\phi_u, \phi_s, \phi_c\}$ must sum to 100% reduces the independent degrees of freedom from 3 to 2. An elegant way to turn this into a "plotting strategy" is to exploit Viviani's theorem: the sum of the shortest distances from any interior point of an equilateral triangle to its sides is constant and equal to the triangle's height. As a corollary, the three symmetric lines radiating out from this point parallel to the triangle's sides can be used to set up coordinates which add up to a fixed number, conveniently chosen as 100%. This is illustrated in Fig. 1 using the point $\phi_u : \phi_s : \phi_c = 20 : 50 : 30$. We can hence represent ternary mixtures as follows: pure components correspond to the corners of the triangle, binary mixtures live on the sides connecting the respective two pure corners, and ternary mixtures are located anywhere in the interior of the triangle.

1.2.2 Typical phase diagram of ternary (and "raft like") lipid mixtures. Let us return to the particular case of ternary mixtures comprising saturated, unsaturated, and cholesterol lipids. Their phase diagram depends of course on the chosen lipids, but at a temperature at which the (pure) saturated lipid is in a gel phase and the (pure) unsaturated lipid in a fluid phase, these diagrams typically take the general form shown in Fig. 1: the *u*- and *s*-lipids exhibit 2-phase coexistence along the binary triangle edge (conventionally picked to be the lower baseline, almost always with "*s*" on the right hand side).

Adding cholesterol (*i.e.*, "moving up"), opens a second 2-phase region near the saturated corner (tie-lines are shown in green) with a cholesterol-poor gel-phase coexisting with a more cholesterol-rich so-called "liquid ordered" (ℓ_o) fluid phase. Both 2-phase regions border at a 3-phase triangle, on whose third side a third 2-phase region is attached. Unlike the other two, it does not extend to its nearest triangle side (namely, *uc*), since at the chosen temperature cholesterol and the unsaturated species mix well (except that cholesterol precipitates at sufficiently high concentration—see below). Instead, the two phases coexisting

Open Access Article. Published on 14 januar 2025. Downloaded on 30-01-2026 17:48:09.
This article is licensed under a Creative Commons Attribution 3.0 Unported Licence.

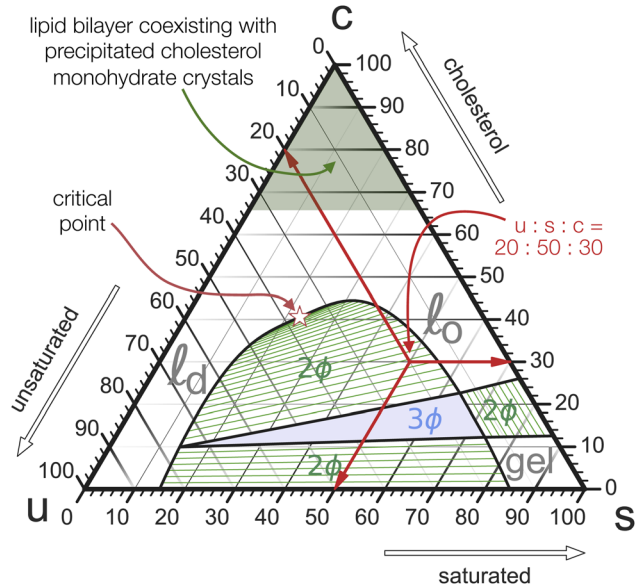

Fig. 1 Gibbs triangle representation of a typical ternary phase diagram of a lipid mixture of saturated, unsaturated, and cholesterol lipids. This image is merely a schematic, but it qualitatively reflects the basic topography measured in many experimental studies. White regions correspond to pure phases, hatched green regions exhibit two-phase coexistence, with the green lines actually being the tie-lines between coexisting phase points. The central blue triangle is a region of three-phase coexistence, in which the pure phases at the triangle's corners coexist. The three red arrows illustrate how to read off the composition of some given point. The sum of their lengths is the same no matter which point in the triangle we pick, which is the key geometric fact that enables this representation in the first place.

across this region—the ℓ_o phase and its "partner", a less ordered (since more unsaturated) "liquid disordered" (ℓ_d) phase, become more similar and merge at a critical point. "Beyond" this point there is no meaningful distinction between a fluid ordered or disordered phase, any more than a meaningful distinction between liquid water and steam can be made past water's critical point—both merely being fluid phases of the same symmetry.

The solubility limit of cholesterol in PC-phospholipids is typically around 66%,[40] above which it precipitates from the bilayer into crystals of cholesterol monohydrate. Once this happens, a point in the Gibbs phase triangle no longer reflects the membrane composition, but the resulting states still feature a stable membrane. In fact, they are experimentally very useful, because they anchor cholesterol's chemical potential to that of its monohydrate, permitting quantitative calibration between different membrane systems.[41]

If the temperature is such that even the saturated lipid is in a fluid phase, then the two gel-fluid coexistence regions vanish from the phase diagram, and with it also the 3-phase triangle. They are effectively "pushed down" to the *us*-binary line and all that survives is the ℓ_o/ℓ_d coexistence. This may look like a very different phase diagram, but recall that gel phases are rarely physiologically relevant. What matters is the fluid–fluid coexistence region and its critical point, which remains

intact, not gel-phase physics created by the pure-*s*-corner. We will subsequently discuss simpler "gel-free" versions of the ternary phase diagram and argue that for the purpose of understanding physiologically interesting ternary lipid mixtures these will suffice.

Open Access Article. Published on 14 januar 2025. Downloaded on 30-01-2026 17:48:09.
This article is licensed under a Creative Commons Attribution 3.0 Unported Licence.

1.3 Membrane asymmetry

Lipid membrane asymmetry is not a recent addition to a biomembrane's complexity list. It was discovered at the very dawn of modern biomembrane science: Mark Bretscher's seminal paper[42] on the subject appeared just 12 days after Singer and Nicholson published their "Fluid Mosaic Model."[43] The following year, Verkleij *et al.* proposed the first rough leaflet distribution in a human red blood cell,[44] followed by similar results from other authors for platelets,[45] the plasma membrane of nucleated cells,[46–48] and some membrane organelles.[49] Recent work by Lorent *et al.*[50] confirmed these early findings and added highly fine-grained detail. Moreover, their bioinformatics analysis of transmembrane proteins anchored by a single-pass α-helix (in particular, that anchor's surface area imbalance) strongly suggests that plasma membrane asymmetry is evolutionarily conserved across all eukarya.

It is worth highlighting that leaflet-specific lipidomes can exist only because spontaneous transitions of phospholipids between leaflets ("flip-flop" events) happen so slowly—between hours and days[51]—that active but slow cellular transmembrane sorting mechanisms can successfully counter the decay into a fully scrambled state. An important exception is cholesterol, whose flip-flop time is believed to be somewhere in the sub-microsecond to millisecond range.[51–54] Hence, its concentration is thermodynamically equilibrated between leaflets on most experimentally and biophysically relevant timescales.

1.3.1 Biological model systems. The most straightforward way to do experiments on asymmetric membranes is to work with those given to us by nature—using live cells, or at least membranes derived from them. A particularly convenient and frequently used model system are so-called giant plasma membrane vesicles (GPMV), which one can obtain by chemically inducing cells to vesiculate (or "bleb").[55–58] In fact, ℓ_o/ℓ_d-like critical fluctuations in biomembranes were first observed in GPMVs.[39]

However, such bio-derived systems as exemplars for asymmetry have a number of drawbacks. The most obvious one is that they are very complicated: they consist of far more than just a few types of lipids, besides also containing many proteins.[58–60] This not only makes it difficult to know (let alone control) their composition; if the goal is to specifically probe asymmetry, their substantial complexity adds numerous confounding factors. Furthermore, it appears that whatever asymmetric composition the plasma membrane has, GPMVs have lost at least some of it (they appear to be at least partially scrambled).[60,61]

1.3.2 Artificially created asymmetric membranes. Clean asymmetric model bilayers are preferable if the goal is to specifically examine asymmetry, but making them has been tricky. This is likely one of the two primary reasons (the other one being the challenge to measure leaflet-resolved properties) why our knowledge of asymmetric membranes lags behind that of symmetric ones, even though we have known basically from day one that the biologically relevant situation is asymmetric.

Open Access Article. Published on 14 januar 2025. Downloaded on 30-01-2026 17:48:09.
This article is licensed under a Creative Commons Attribution 3.0 Unported Licence.

Luckily, this situation has changed dramatically over the past decade: by now more than 70 protocols for synthesizing asymmetric bilayers have been published, which Krompers and Heerklotz have recently reviewed, classified into four major categories, and analyzed in terms of advantages and drawbacks.[62] We believe that the availability of such clean model systems is a key driver of asymmetry's renaissance. And yet, the community has only just begun to explore the exciting opportunities this affords. This includes many now feasible research questions that are waiting to be realized, likely offering consequential insights into the biological situation.

1.3.3 Types of asymmetry. A leaflet-specific lipid content is the most salient aspect of membrane asymmetry, but it is by no means the only one. In fact, if we break the symmetry of one specific observable (here: composition), other symmetries are prone to break in the process. The generic assumption should therefore be that any observable that can be defined at the leaflet level is symmetry broken once one such observable is symmetry broken. This could be structural properties (*e.g.*, area per lipid, thickness, charge density), mechanical properties (*e.g.*, elastic moduli, spontaneous curvature, leaflet tensions and torques), or dynamical ones (*e.g.*, diffusion constant, viscosity, relaxation rates). In this paper, we will focus—besides the obvious compositional degree of freedom—on two mechanical observables: differential stress, $\Delta\Sigma$, and bilayer torque, $\mathscr{T}$.

Differential stress is the difference between the two individual mechanical leaflet tensions,

$$\Delta\Sigma = \Sigma_+ - \Sigma_-, \tag{1}$$

where we use "+" and "−" to distinguish the two leaflets, which we henceforth will refer to as "leaf$_+$" and "leaf$_-$" (think of "+" as the "upper" or "outer" one, if you wish). Differential stress $\Delta\Sigma$ is the "orthogonal partner" to the more common total tension $\Sigma = \Sigma_+ + \Sigma_-$, in the sense that these two observables define a new set of orthogonal axes in the leaflet-resolved tension space $\{\Sigma_+, \Sigma_-\}$. Our group has pointed out that differential stress must be included when discussing membrane asymmetry; in fact, since often $\Delta\Sigma \gg \Sigma$, it can be the more important variable.[63–67]

Bilayer torque $\mathscr{T}$ is the thermodynamic observable conjugate to a membrane's extrinsic curvature J, *i.e.*, the (generalized) force that drives bending,

$$\mathscr{T} = \left(\frac{\partial f}{\partial J}\right)_{T,\Sigma,\ldots}, \tag{2}$$

where f is the free energy per area and the subscripts remind us which other observables are meant to remain fixed.

Differential stress can be rephrased as the existence of a preferred bilayer curvature $J_{0,s}$ at which this stress vanishes, because at fixed lipid content bending changes the leaflet reference areas measured some distance z_0 away from the bilayer midsurface, to lowest order linear in the curvature. (The relevant reference surface at this distance z_0 is the so-called "neutral surface," at which bending and stretching energies decouple.) This implies that we should be able to write[63]

$$\Delta\Sigma = \frac{\kappa_{\mathrm{nl}}}{z_0}(J - J_{0,s}), \tag{3}$$

Open Access Article. Published on 14 januar 2025. Downloaded on 30-01-2026 17:48:09.
This article is licensed under a Creative Commons Attribution 3.0 Unported Licence.

where $\kappa_{\mathrm{nl}} \simeq K_{\mathrm{A}} z_0^2$ and K_{A} is a membrane's area expansion modulus. We can then combine bending and differential stress into a single curvature-elastic expression of the form[63–67]

$$f = \frac{1}{2}\kappa(J - J_{0,\mathrm{b}})^2 + \frac{1}{2}\kappa_{\mathrm{nl}}(J - J_{0,\mathrm{s}})^2, \tag{4}$$

where κ is the ordinary bending modulus and $J_{0,\mathrm{b}}$ the more common lipid-shape based spontaneous bilayer curvature. The torque is hence

$$\mathscr{T} = \left(\frac{\partial f}{\partial J}\right)_{T,\Sigma,\ldots} = \underbrace{\kappa(J - J_{0,\mathrm{b}})}_{\mathscr{T}_\kappa} + \underbrace{\kappa_{\mathrm{nl}}(J - J_{0,\mathrm{s}})}_{\mathscr{T}_\Sigma} \tag{5a}$$

$$\overset{(3)}{=} \kappa(J - J_{0,\mathrm{b}}) + z_0 \Delta\Sigma. \tag{5b}$$

Fig. 2 illustrates the sign conventions for these two terms.

Demanding that a flat membrane is torque free (*i.e.*, it will voluntarily stay flat) yields

$$0 = \mathscr{T}(J = 0) \overset{(5b)}{=} -\kappa J_{0,\mathrm{b}} + z_0 \Delta\Sigma \quad \Rightarrow \quad \Delta\Sigma = \frac{\kappa J_{0,\mathrm{b}}}{z_0}. \tag{6}$$

Using common values on the right hand side (such as $\kappa \simeq 30 k_{\mathrm{B}}T$, $J_{0,\mathrm{b}} \simeq$ few $\times 10^{-2}$ mN m^{-1}, and $z_0 \simeq 1$ nm) shows that we should expect $\Delta\Sigma$ to be on the order of a few mN m^{-1}, which is between one and two orders of magnitude larger than typical cellular membrane tensions.[68]

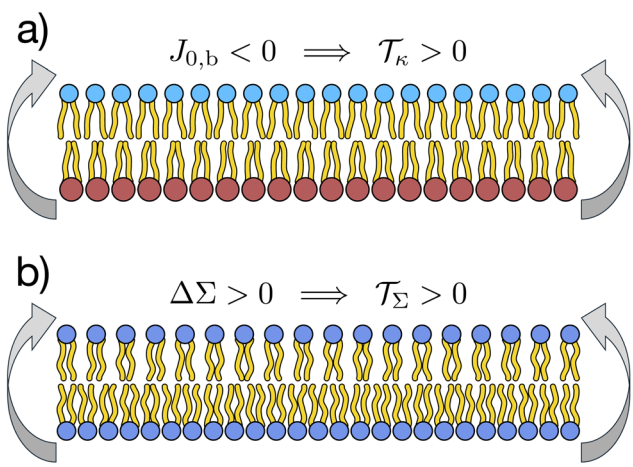

Fig. 2 Clarifying the sign of the torque, $\mathscr{T} = \mathscr{T}_\kappa + \mathscr{T}_\Sigma$. (a) The torque due to lipid curvature, $\mathscr{T}_\kappa$, strives to bend the membrane up when the spontaneous bilayer curvature is negative, $J_{0,\mathrm{b}} < 0$, *i.e.* when the upper leaflet has a more negative spontaneous curvature than the lower one. (b) The torque due to differential stress, $\mathscr{T}_\Sigma$, strives to bend the membrane up when the differential stress is positive, $\Delta\Sigma > 0$, *i.e.* when the upper leaflet is under excess tension.

Open Access Article. Published on 14 januar 2025. Downloaded on 30-01-2026 17:48:09.
This article is licensed under a Creative Commons Attribution 3.0 Unported Licence.

2 Towards ternary asymmetric phase diagrams

Whatever the precise physics of asymmetric ternary lipid mixtures will be, it is clear that these systems have more degrees of freedom than their symmetric counterparts—most obviously since we now have to deal with two nontrivial leaflet compositions. This means that we will not merely be asking how the phases in a diagram such as the one in Fig. 1 might change. The more profound question is: what type of phase diagrams should we be drawing in the first place? What are good thermodynamic variables to put on the axes of what kind of plot? How many degrees of freedom do we have, and what are they?

2.1 Effective binary modeling

So far experiments offer little guidance, since leaflet-resolved phase diagrams are practically nonexistent. The first (and so far only) measurement of a leaflet-resolved *binary* phase diagram (a mixture of two phospholipids, DOPC and DPPC) was only published in 2023.[69] While experimentally challenging, it is conceptually straightforward: the mole-fraction on each side is a single number, which yields a straightforward two-dimensional diagram for which theoretical predictions exist.[70–72] Ternary lipid systems have also been studied theoretically, but the cholesterol component has been treated implicitly, essentially by considering a single order parameter that distinguishes ℓ_o from ℓ_d (rendering the problem effectively that of a binary mixture), to which a rapidly flip-flopping cholesterol component is locked.[70–75] At any rate, differential stress or considerations regarding torque have not been part of any analysis.

2.2 Counting degrees of freedom

2.2.1 Simplistic counting gives 4 degrees of freedom. Let us count the degrees of freedom to establish the dimensionality of the problem. Each leaflet is a ternary mixture, which has a two-dimensional phase-space—one Gibbs triangle for each side. A convenient way to parametrize points in those is *via* the following two coordinates. First, define leaflet-specific saturation ratios

$$r_{\pm} = \frac{S_{\pm}}{U_{\pm} + S_{\pm}} \equiv \frac{S_{\pm}}{L_{\pm}}, \tag{7}$$

which measure the relative percentage of saturated phospholipids $S_{\pm}$ among all phospholipids $L_{\pm} = U_{\pm} + S_{\pm}$. States of constant $r_{\pm}$ form lines that pass through the cholesterol corner and divide the opposite *us*-side at the respective ratio of *s*-lipids. Second, to single out a point on that line, we may specify its cholesterol mole fraction, which we will henceforth denote with the symbol $\phi_{\pm}$. These coordinates are illustrated in Fig. 3. Since both Gibbs triangles parametrize two-dimensional phase spaces, the total problem appears to have 4 degrees of freedom.

2.2.2 More careful counting also gives 4 degrees of freedom. Four degrees of freedom is in fact the correct answer, but to properly understand why, we need to account for two additional and very important effects—one which will remove a degree of freedom, and another one which will add a degree of freedom.

First the removal. Since cholesterol rapidly flip-flops between the leaflets, we need to satisfy the condition of equal chemical potential,

Open Access Article. Published on 14 januar 2025. Downloaded on 30-01-2026 17:48:09.
This article is licensed under a Creative Commons Attribution 3.0 Unported Licence.

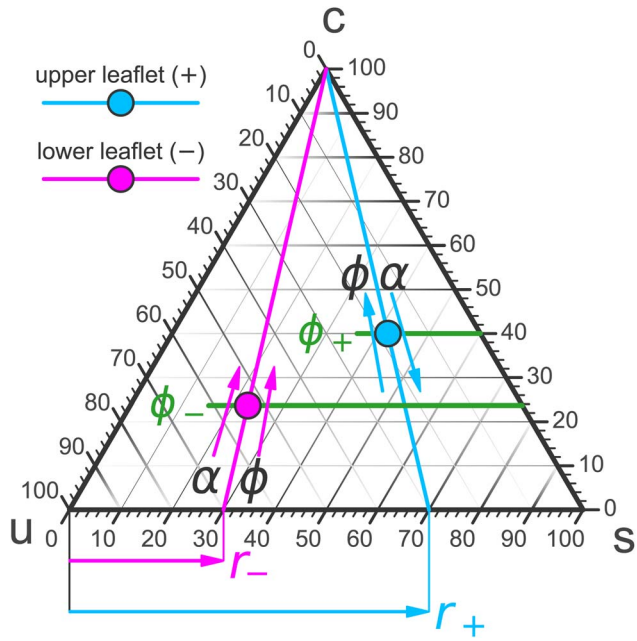

Fig. 3 Parametrizing points in a ternary lipid mixture *via* the saturation ratios $r_\pm$ and the cholesterol mole fractions $\phi_\pm$. The two colors correspond to compositions in the two leaflets—cyan being leaf$_+$, magenta leaf$_-$. The arrows next to the two leaflet compositions indicate how each would respond to an increase in either the total cholesterol content ϕ or the phospholipid leaflet abundance α.

$$\mu^{+}_{\mathrm{chol}} = \mu^{-}_{\mathrm{chol}}. \tag{8}$$

This constraint reduces the number of degrees of freedom from 4 to 3. The cholesterol fractions ϕ_+ and ϕ_- in the two leaflets cannot be set to whatever values we desire; instead, we can only decide on the total mole fraction ϕ of cholesterol, defined *via*

$$\phi = \frac{C_+ + C_-}{L_+ + L_- + C_+ + C_-} \equiv \frac{C}{L + C} \equiv \frac{N_+\phi_+ + N_-\phi_-}{N_+ + N_-}, \tag{9}$$

where $N_\pm$ are the total lipid numbers in each leaflet. As cholesterol equalizes its chemical potential on both sides *via* flip-flop, the individual coexisting leaflet fractions $\phi_\pm$ arise.

Now the addition. Compositional ternary diagrams such as the one in Fig. 1 only record mole fractions; they know nothing about the absolute number of lipids on the two different sides. It proves useful to include this missing thermodynamic information not *via* the individual lipid numbers $N_\pm$ but in terms of total lipid content, $N_+ + N_-$, and number difference, $N_+ - N_-$. The former captures potentially interesting physics pertaining to system size (which we will sidestep in this paper), while the latter homes in more directly on asymmetry. Considering that cholesterol rapidly flip-flops, it is more convenient to specify the abundance asymmetry *via* the phospholipid contingent, which does not change under

Open Access Article. Published on 14 januar 2025. Downloaded on 30-01-2026 17:48:09.
This article is licensed under a Creative Commons Attribution 3.0 Unported Licence.

cholesterol redistribution; let us hence define the phospholipid abundance asymmetry

$$\alpha = \frac{L_+ - L_-}{L_+ + L_-}. \tag{10}$$

In the absence of cholesterol, changing the abundance by $\Delta\alpha$ changes the differential stress by $\Delta\Delta\Sigma = -K_A\Delta\alpha$ (assuming area additivity, since abundance then couples directly to area difference, the observable conjugate to differential stress). Shifting α by just a few percentage points would then change differential stress by several mN m^{-1}, rendering α a fairly "stiff" degree of freedom.

We will see that once cholesterol is present, its ability to offset a phospholipid imbalance by redistributing into the less crowded leaflet permits much larger changes of α without incurring huge differential stress. Of note, recent experiments have claimed that the cytosolic leaflet of the human red blood cell contains about twice as many phospholipids as the exoplasmic one (*i.e.*, $\alpha \sim -33\%$),[76] in line with the raw data of no less than five previous studies (see Table S1 in that reference). Such an enormous abundance asymmetry would profoundly affect cholesterol distribution and leaflet-specific phase behavior, both fields rife with their own controversial claims. We expect that further work dedicated to this complex interplay has the potential to resolve numerous contentious issues. Our goal here is to develop a theoretical framework that accounts for phospholipid abundance asymmetry, however large it may prove to be, such that its thermodynamic implications can be quantitatively examined.

2.2.3 Using ϕ and α to independently tune ϕ_+ and ϕ_-. Having leaflet abundance as a new tuning knob, a fascinating possibility emerges: despite the fact that we cannot pick two values ϕ_+ and ϕ_- for the cholesterol leaflet mole fractions and expect them to automatically stay that way, we might be able to make them coexist by a suitable choice of cholesterol fraction ϕ and phospholipid abundance α. The reason is that these two tuning parameters drive linearly independent responses in the cholesterol leaflet fractions $\phi_\pm$. Consider again Fig. 3: if we increase ϕ, we expect both leaflet fractions $\phi_\pm$ to also increase; likewise, a decrease in ϕ entails decreases in $\phi_\pm$. But the response to changes in α is very different: if we increase α (at fixed total tension), then we put leaf$_+$ under compression and leaf$_-$ under tension. As a result, we will "squeeze" cholesterol from leaf$_+$ to leaf$_-$ and hence decrease ϕ_+ while simultaneously increasing ϕ_-.

Small changes in ϕ and α trigger small changes in the $\phi_\pm$, which are presumably linear. This shows that

$$\begin{pmatrix} \Delta\phi_+ \\ \Delta\phi_- \end{pmatrix} = \begin{pmatrix} a_{11} & -a_{12} \\ a_{21} & a_{22} \end{pmatrix} \begin{pmatrix} \Delta\phi \\ \Delta\alpha \end{pmatrix} \tag{11}$$

with positive numbers a_{ij}. These depend on ϕ and α (and other parameters of the problem), and they are not entirely independent, since conservation of the total cholesterol content linearly couples $\Delta\phi_+$ and $\Delta\phi_-$ (in some cumbersome way). All the same, the "parallel" and "antiparallel" responses to changes in ϕ and α add the minus sign to the upper right entry of the matrix in eqn (11), which guarantees that it is invertible. Hence, if we wish to make a specific (small) change in the

Open Access Article. Published on 14 januar 2025. Downloaded on 30-01-2026 17:48:09.
This article is licensed under a Creative Commons Attribution 3.0 Unported Licence.

cholesterol leaflet fractions, the required adjustments of cholesterol content and abundance asymmetry are

$$\begin{pmatrix} \Delta\phi \\ \Delta\alpha \end{pmatrix} = \frac{1}{a_{11}a_{22} + a_{12}a_{21}} \begin{pmatrix} a_{22} & a_{12} \\ -a_{21} & a_{11} \end{pmatrix} \begin{pmatrix} \Delta\phi_+ \\ \Delta\phi_- \end{pmatrix}. \tag{12}$$

To be clear: we are not guaranteed that we can always make every conceivable pair $\{\phi_+, \phi_-\}$ coexist, since this local argument does not clarify global reach. Besides the fact that cholesterol does not dissolve in a membrane beyond $\sim$66%,[40,41] permissible $\Delta\phi$ and especially $\Delta\alpha$ will have feasibility limits of their own. Additionally, edge cases are likely problematic. For instance, it will be impossible to make a nonzero ϕ_+ coexist with a vanishing ϕ_-, because mixing entropy terms of the form $\phi \log \phi$ will create an infinite driving force at $\phi \to 0$ that cannot be balanced by any finite enthalpic terms.

To summarize the present discussion: we have argued that the thermodynamic phase space of our system is four-dimensional—already disregarding "obvious" variables such as the total number of lipids $N = N_+ + N_-$ (*i.e.*, the system size) and the temperature T, both of which we imagine fixed once and for all. Possible independent degrees of freedom are $\{r_+, r_-, \phi_+, \phi_-\}$ or alternatively $\{r_+, r_-, \phi, \alpha\}$. The former can be easily visualized as two points in a ternary phase diagram, and realizing them requires a judicious choice of ϕ and α. The latter may be more easily tunable experimentally and yield leaflet-specific cholesterol fractions ϕ_+ and ϕ_- that arise after flip-flop assisted chemical potential equilibration.

2.3 Some important new linear response functions

The matrix elements in eqn (11) describe the local linear relation for how $\{\phi_+, \phi_-\}$ vary with $\{\phi, \alpha\}$. In other words, they quantify the *linear response* of the leaflet cholesterol fractions to the external control parameters of cholesterol content and phospholipid abundance.

More generally, we can define susceptibilities that measure the response to changes in external control variables—as is routinely done in thermodynamics. For now, let us focus on responses to changing $\{\phi, \alpha\}$, which are most closely related to the question of asymmetry and ternary mixtures, even though we could also include $\{r_+, r_-\}$ into the mix.

The observables whose perturbation we will discuss in a bit more detail here are differential stress $\Delta\Sigma$ and bilayer torque $\mathscr{T}$, so let us define their α-related susceptibilities

$$\chi^{\Delta\Sigma}_{\alpha|\phi}(\phi,\ \alpha,\ r_+,\ r_-,\ T,\ N,\ J,\ \ldots) = -\left(\frac{\partial\Delta\Sigma}{\partial\alpha}\right)_{\phi,r_+,r_-,T,N,J,\ldots} \tag{13a}$$

$$\chi^{\mathscr{T}}_{\alpha|\phi}(\phi,\ \alpha,\ r_+,\ r_-,\ T,\ N,\ J,\ \ldots) = -\left(\frac{\partial\mathscr{T}}{\partial\alpha}\right)_{\phi,r_+,r_-,T,N,J,\ldots}, \tag{13b}$$

as well as their ϕ-related partners

$$\chi^{\Delta\Sigma}_{\phi|\alpha}(\phi,\ \alpha,\ r_+,\ r_-,\ T,\ N,\ J,\ \ldots) = \left(\frac{\partial\Delta\Sigma}{\partial\phi}\right)_{\alpha,r_+,r_-,T,N,J,\ldots} \tag{13c}$$

$$\chi^{\mathscr{T}}_{\phi|\alpha}(\phi,\ \alpha,\ r_+,\ r_-,\ T,\ N,\ J,\ \ldots) = \left(\frac{\partial \mathscr{T}}{\partial \phi}\right)_{\alpha,r_+,r_-,T,N,J,\ldots}. \tag{13d}$$

These would almost surely benefit from easier notations (at least this one is informative), as well as some intuitive names, since cumbersome attempts like "iso-compositional differential stressability" for $\chi^{\Delta\Sigma}_{\alpha|\phi}$ are not likely to catch on. Nevertheless, as linear response functions they satisfy the joint differential relation

$$\begin{pmatrix} \mathrm{d}\mathscr{T} \\ \mathrm{d}\Delta\Sigma \end{pmatrix} = \begin{pmatrix} -\chi^{\mathscr{T}}_{\alpha|\phi} & \chi^{\mathscr{T}}_{\phi|\alpha} \\ -\chi^{\Delta\Sigma}_{\alpha|\phi} & \chi^{\Delta\Sigma}_{\phi|\alpha} \end{pmatrix} \begin{pmatrix} \mathrm{d}\alpha \\ \mathrm{d}\phi \end{pmatrix}, \tag{14}$$

which also implies that they obey the obvious Maxwell relations

$$\frac{\partial}{\partial\alpha}\chi^{\mathscr{T}}_{\phi|\alpha} = -\frac{\partial}{\partial\phi}\chi^{\mathscr{T}}_{\alpha|\phi} \quad \text{and} \quad \frac{\partial}{\partial\alpha}\chi^{\Delta\Sigma}_{\phi|\alpha} = -\frac{\partial}{\partial\phi}\chi^{\Delta\Sigma}_{\alpha|\phi}. \tag{15}$$

While it might be difficult to determine these susceptibilities quantitatively in experiment, they will all have a noticeable impact on the response of vesicles, especially micron-scale giant unilamellar vesicles (GUVs), to the respective changes (see Section 3 below). At the very least, their signs would be straightforward to observe, and possibly even whether the response is "strong" or "mild". Of course, in simulations they are very accessible, and we will discuss some examples below.

Let us elaborate on the sign. We expect the susceptibilities with respect to changes in α to have a definite sign, because α itself has a definite sign baked into it. Recall that increasing α means that we will increase the phospholipid content in leaf$_+$ relative to leaf$_-$. This will put leaf$_+$ under compression and leaf$_-$ under tension. Since stress is the negative of pressure, this change will make the derivative $\partial\Delta\Sigma/\partial\alpha$ negative, and for that reason we propose the extra minus sign in the definition of $\chi^{\Delta\Sigma}_{\alpha|\phi}$, which would then render it positive. A similar argument explains the extra minus sign in the definition of $\chi^{\mathscr{T}}_{\alpha|\phi}$: pushing more phospholipids into leaf$_+$ gives rise to a torque that would drive "down-bending" (*i.e.*, leaf$_+$ will bulge "out"), and from eqn (5b) or (6) it is clear that this corresponds to a negative torque, which the extra minus sign then turns into a positive susceptibility.

The situation is slightly more subtle, though, because in the presence of cholesterol the membrane can relax the differential stress induced by a change in α by cholesterol relocation from the compressed to the tense leaflets. The same holds for the torque: its change, too, will be curtailed by cholesterol flip-flop. Unless this cholesterol relocation triggers a compositional instability (which might happen if we push one side into a phase coexistence region), we would expect it to reduce the changes in $\Delta\Sigma$ or $\mathscr{T}$ (compared to the cholesterol-free case), but not to actually flip the sign. This is not a rigorous argument, though.

Importantly, the response functions with respect to cholesterol, $\chi^{\Delta\Sigma}_{\phi|\alpha}$ and $\chi^{\mathscr{T}}_{\phi|\alpha}$, behave very differently. If we increase ϕ, this neither means that cholesterol will increase in a specific leaflet, nor does it distribute in equal amounts between the two leaflets (even though it will distribute such that $\mu_{\mathrm{chol}}{}^{+} = \mu_{\mathrm{chol}}{}^{-}$ remains true). Consider the following illustrative scenarios:

Open Access Article. Published on 14 januar 2025. Downloaded on 30-01-2026 17:48:09.
This article is licensed under a Creative Commons Attribution 3.0 Unported Licence.

Open Access Article. Published on 14 januar 2025. Downloaded on 30-01-2026 17:48:09.
This article is licensed under a Creative Commons Attribution 3.0 Unported Licence.

(1) A cholesterol-free compositionally symmetric membrane is under some lipid abundance asymmetry $\alpha > 0$. If we add cholesterol, the chemical partitioning forces are equal, but the differential stress $\Delta\Sigma$ due to α will guide cholesterol preferentially into the leaflet whose tension is larger, thus reducing the magnitude of $\Delta\Sigma$. This will render $\chi^{\Delta\Sigma}_{\phi|\alpha}$ negative if the differential stress is positive and positive if the differential stress is negative.

(2) A compositionally asymmetric membrane is under vanishing differential stress. If we add cholesterol, there is no driving force coming from the stress, but the compositional difference will now bias cholesterol—away from the phase that already contains a higher mole fraction of cholesterol but also towards the side into which cholesterol partitions better (say, the more saturated one). The resulting change in differential stress—and hence the sign of $\chi^{\Delta\Sigma}_{\phi|\alpha}$—can be either positive or negative, depending on how these drivers pan out.

We have previously observed both of these cases in simpler binary systems.[77] Notice that the undetermined sign of $\chi^{\Delta\Sigma}_{\phi|\alpha}$, rather than being annoying, means that the mere *direction* of an effect will be informative about some conceivably difficult to ascertain membrane observables—such as, is there a cholesterol imbalance between the leaflets, or is there pre-existing differential stress. Experiments that change ϕ might thus be very informative.

We expect the situation for $\chi^{\mathscr{T}}_{\phi|\alpha}$ to be similar: the sign is not pre-determined and instead depends on the specifics of the underlying situation. It is unfortunately more difficult to make analogous arguments, because the response of cholesterol's inter-leaflet distribution to changes in torque are more subtle. The differential stress contribution to the torque, $\mathscr{T}_\Sigma = z_0\Delta\Sigma$ is of course the same, but the part of the torque due to lipid shape, $\mathscr{T}_J = -\kappa J_{0,\mathrm{b}}$, requires an answer to the question how $J_{0,\mathrm{b}}$ changes with cholesterol concentration—a famously tricky problem that might not be simply captured by a linear combination of some "bare" intrinsic lipid curvatures.[78–80] It seems to us that a workable rule of thumb is that at sufficiently large cholesterol content, any further increase will tend to reduce the magnitude of torque. One way of seeing this is that in the "theorist's limit" of $\phi \to 1$ we reach a perfectly symmetric membrane, which hence has zero torque (and also zero differential stress). The "ultimate" direction into which $\mathscr{T}$ must change as ϕ increases is hence clear, even though at intermediate concentrations additional drivers may well complicate matters. (Of course, the same argument can be made for the differential stress.)

2.4 Zero torque foliations

After identifying a set of variables that specify the thermodynamic state, all other observables will be functions of those. For instance, if we initially pick two desired leaflet compositions $\{r_-, \phi_-\}$ and $\{r_+, \phi_+\}$, then the $\{\phi, \alpha\}$ values needed to realize them are functions of those. Likewise, observables such as differential stress, $\Delta\Sigma$, or bilayer torque, $\mathscr{T}$, are now set, and neither of them is generally zero. For the differential stress that is intuitively easy to see: two arbitrarily chosen leaflet compositions generally do not coexist in their cholesterol content across the leaflets. To prevent a net flux from one leaflet to the other, we need to set up a stress difference that opposes such a translocation.

Let us follow this idea a bit further. Pick a composition $\{r_-, \phi_-\}$ for leaf$_-$ (the magenta point in Fig. 4) and try to arrange for chemical coexistence with

Open Access Article. Published on 14 januar 2025. Downloaded on 30-01-2026 17:48:09.
This article is licensed under a Creative Commons Attribution 3.0 Unported Licence.

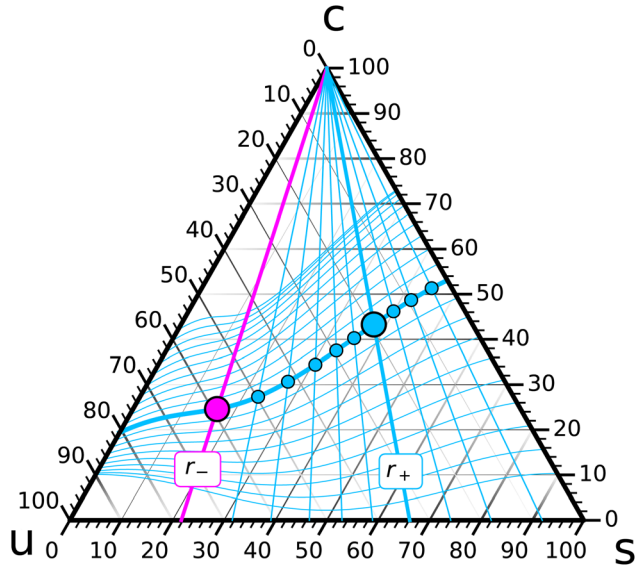

Fig. 4 Schematic illustration of a zero torque foliation. A given composition $\{r_-, \phi_-\}$ in leaf$_-$ (magenta point) can be made to coexist with a wide range of $\{r_+, \phi_+\}$ compositions in leaf$_+$, but at a specified r_+ value (say, the bold cyan line) only a small number of ϕ_+ values (likely only a single one, the big cyan point) will additionally coexist at zero torque $\mathscr{T}$. The collection of all such points over a range of r_+ values forms a one-dimensional slice of zero-torque states through the ternary diagram. The family of all such curves, parametrized by different ϕ_- values on the r_- line of leaf$_-$, constitute a foliation of the ternary phase diagram. (The specific one shown here is merely for illustration; it is not based on a particular free energy model.)

compositions in leaf$_+$ that have a fixed saturation ratio r_+ but different values of ϕ_+ (points on the bold cyan r_+ line in Fig. 4). Each such point will require some specific $\{\phi, \alpha\}$ combination, and once we have found it, it will result in a bilayer with some differential stress, and some torque, whose value depends on ϕ_+:

$$\Delta\Sigma(\phi_+) = \Delta\Sigma(\phi_+|r_-, \phi_-, r_+), \tag{16a}$$

$$\mathscr{T}(\phi_+) = \mathscr{T}(\phi_+|r_-, \phi_-, r_+). \tag{16b}$$

Consider for instance the torque: the function $\mathscr{T}(\phi_+)$ varies with ϕ_+ in some conceivably complicated and yet-to-be-determined way, and for some value of ϕ_+ it might vanish (the cyan point on the bold cyan r_+ line in Fig. 4). At this special point the two ternary compositions in the two leaflets do not just chemically coexist; they coexist at zero torque, which constitutes an additional mechanical condition. Constraint counting of this type does not answer the question how many solutions $\mathscr{T}(\phi_+) = 0$ has. However, in light of the underlying physical situation we expect this equation to identify a small number of points along the r_+ curve, likely just a single one, that coexist with the composition $\{r_-, \phi_-\}$ at vanishing bilayer torque.

Open Access Article. Published on 14 januar 2025. Downloaded on 30-01-2026 17:48:09.
This article is licensed under a Creative Commons Attribution 3.0 Unported Licence.

Let us now also vary the r_+ line, and for each one find the special zero-torque-point(s) on it (a few are illustrated as smaller cyan points in Fig. 4). Their collection forms a one-dimensional curve in the ternary phase diagram, namely, the locus of all leaflet compositions in leaf$_+$ that can coexist at vanishing torque with the given point $\{r_-, \phi_-\}$ in leaf$_-$. This curve has to pass through the $\{r_-, \phi_-\}$ point, because this gives rise to a symmetric bilayer, and we know that such a system would also have zero torque.

Finally, we can construct such zero-torque-curves for any cholesterol fraction ϕ_- on the r_- line. This yields a foliation of the ternary phase diagram into zero torque coexistence curves: a specified composition $\{r_-, \phi_-\}$ in leaf$_-$ can in principle coexist with any composition $\{r_+, \phi_+\}$ in leaf$_+$ (a set of dimension two), but only a one-dimensional subset $\phi_+(r_+|r_-, \phi_-)$ coexists at zero torque.

We hasten to clarify that the zero-torque-curves we constructed depend on the points $\{r_-, \phi_-\}$ in leaf$_-$ to which we pinned them. We are not claiming that any two points selected on a given curve will coexist with one another at zero torque—this is a stronger condition that does not follow from the simple counting argument we have presented.

3 Zero torque states and their perturbations

We concluded the previous section by specifically discussing a coexistence between the two leaflets that ensures a vanishing torque. Why is this interesting?

3.1 Stability of giant unilamellar vesicles

There is no reason why compositionally asymmetric membranes should be flat: we have broken the reflection symmetry of a membrane (with respect to its midplane) in terms of chemical identity, so we should expect that membrane shape itself also fails to obey that symmetry: it will generally be curved—meaning, it will be driven into a curved state by a nonzero torque $\mathscr{T}$. Let us estimate how much curvature we should expect. If the membrane is free of any additional stresses (especially differential stress) then its spontaneous bilayer curvature should be the difference of the individual spontaneous leaflet curvatures $J_{0,\mathrm{m}\pm}$, weighted by their respective monolayer bending rigidities $\kappa_{\mathrm{m}\pm}$:

$$J_{0,\mathrm{b}} = \frac{\kappa_{\mathrm{m}+}J_{0,\mathrm{m}+} - \kappa_{\mathrm{m}-}J_{0,\mathrm{m}-}}{\kappa_{\mathrm{m}+} + \kappa_{\mathrm{m}-}} \approx \frac{1}{2}(J_{0,\mathrm{m}+} - J_{0,\mathrm{m}-}). \tag{17}$$

Considering the $J_{0,\mathrm{m}}$ values of typical lipids,[81] equilibrium radii $R_{0,\mathrm{b}} = 2/J_{0,\mathrm{b}}$ of asymmetric vesicles are usually on the order of a few tens of nanometers (the size of small unilamellar vesicles, SUVs), unless we pick two lipid species that just happen to have very similar spontaneous curvatures. However, many techniques have been developed to create asymmetric giant unilamellar vesicles (GUVs),[62] whose curvature radii are easily two orders of magnitude larger than those of SUVs. Why are they stable against submicroscopic tubulation?

A possible answer is that despite the large spontaneous bilayer curvature $J_{0,\mathrm{b}}$ originating from the lipid shape asymmetry, the net torque is actually very small, because a counter-torque arising from differential stress cancels the spontaneous curvature torque.[63,64,66,67] As we argued following eqn (6), this would mean that an

Open Access Article. Published on 14 januar 2025. Downloaded on 30-01-2026 17:48:09.
This article is licensed under a Creative Commons Attribution 3.0 Unported Licence.

asymmetric flat membrane—and hence, essentially any asymmetric GUV—has to experience a differential stress of a few mN m^{-1}.

Conversely, that asymmetric GUVs should have $\mathscr{T} \simeq 0$ implies that the zero torque foliations discussed in Section 2.4 become constraints on the compositions that may coexist across a GUV's leaflet: once the composition on one side is fixed, the composition on the other is limited to a one-dimensional slice through the ternary phase diagram.

As an example: we propose that the $\mathscr{T} = 0$ constraint will fix the abundance asymmetry of GUVs during their creation. The precise mechanism is likely complicated and will depend on the protocol for making asymmetric GUVs in the first place, but our stability argument sidesteps such details and simply notes the following: if the saturation ratios $\{r_+, r_-\}$ are set, then all that needs to be determined are the $\{\phi_+, \phi_-\}$ values, *via* suitable choices of $\{\phi, \alpha\}$. However, the condition $\mathscr{T} = 0$ selects a one-dimensional subset from those. For instance, if the asymmetric creation protocol somehow fixes ϕ, then the condition $\mathscr{T} = 0$ sets α, because any other choice of α would not produce a GUV that is mechanically stable against tubulation. Almost the same argument holds if the creation process instead fixes ϕ_-. The very existence of a stable asymmetric GUV means that we must have achieved torque balance, and whatever compositional arrangements materialized, there is only one corresponding α that will do so.

3.2 Perturbing cholesterol content and abundance

Since perturbations of a vesicle's thermodynamic state need not keep the two leaflet compositions on the same zero-torque-foliation, we expect that they trigger shape deformations—anywhere from mild ones such as sphere → prolate → oblate → stomatocyte,[82,83] up to the formation of membrane tubules.[84–87] Let us discuss two specific examples, related to changes of ϕ and α.

3.2.1 Changing cholesterol content. Consider two leaflet compositions $\{r_-, \phi_-\}$ and $\{r_+, \phi_+\}$ coexisting in a mechanically stable asymmetric GUV—such as the filled magenta and cyan circles sharing the same bold cyan zero-torque foliation curve in Fig. 5. Let us now change the cholesterol content of the membrane. Experimentally, this is commonly achieved with the help of an exchange agent such as methyl-β-cyclodextrin (MβCD).[88–90] Briefly, cyclodextrins are water soluble cyclic oligosaccharides which posses hydrophobic cavities that can transport small hydrophobic molecules across aqueous environments. If we for instance expose GUVs to "empty" MβCD, it will extract cholesterol from the outer leaflet it has access to, but since cholesterol molecules in both leaflets are in chemical equilibrium, we effectively remove them from both leaflets—meaning, we lower ϕ, to an extent dependent on the details of MβCD exposure. In practice, the situation is a bit more complicated, though, because MβCD can also exchange phospholipids. For instance, Rahimi *et al.*[91] have conducted experiments like those we propose here, aiming to add cholesterol to vesicles *via* pre-loaded MβCD, and found that discharged MβCD can in turn remove phospholipids from the outer leaflets of their GUVs. To avoid this, one should restrict to MβCD concentrations too low to noticeably extract phospholipids.[92]

Lowering ϕ will reduce the cholesterol leaflet concentrations $\phi_\pm$, even though not necessarily by the same amount. More importantly, we generally have no guarantee that the two new points will still share a zero-torque foliation curve.

Open Access Article. Published on 14 januar 2025. Downloaded on 30-01-2026 17:48:09.
This article is licensed under a Creative Commons Attribution 3.0 Unported Licence.

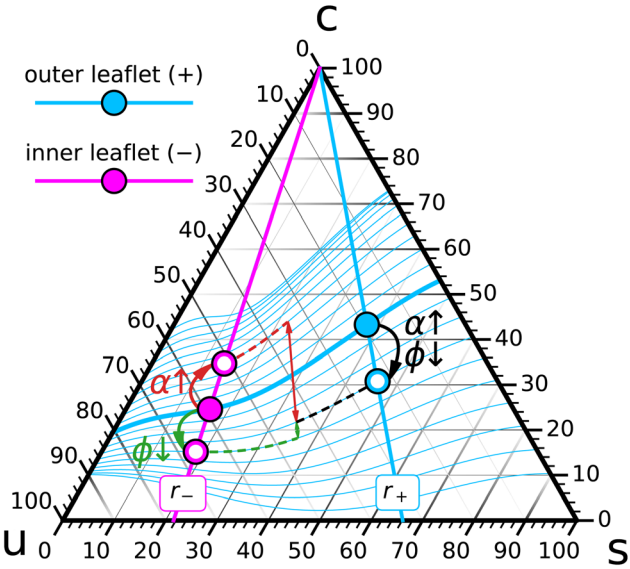

Fig. 5 Perturbation of a ternary asymmetric GUV initially set up such that its inner composition $\{r_-, \phi_-\}$ (big magenta dot) and outer composition $\{r_+, \phi_+\}$ (big cyan dot) chemically coexist at $\mathscr{T} = 0$. The two independent perturbations which either decrease ϕ or increase α will have a similar effect on leaf$_+$: a reduction of ϕ_+. But their effects on leaf$_-$ are opposite: depleting cholesterol will reduce ϕ_- while increasing α will increase ϕ_-. The extent to which this moves points that originally shared the same zero-torque foliation onto different foliation curves is very different.

Stated in terms of the response functions defined in Section 2.3, there is no reason to believe the susceptibility $\chi^{\mathscr{T}}_{\phi|\alpha}$ vanishes (we will see it might, but only for very special conditions). As a consequence, we expect that the GUV would want to deform—if it can. Deflated GUVs should therefore have a tendency to assume new shapes, and since the shape diagrams for deflated vesicles are well understood,[82,83] the nature of these deformations will alert us at the very least to the sign of $\chi^{\mathscr{T}}_{\phi|\alpha}$ under the present conditions.

3.2.2 Changing phospholipid abundance. Consider the same two coexisting points we just studied in Section 3.2.1, but instead of depleting the system of cholesterol, we now add a small amount of phospholipids to the outer side (to be specific: leaf$_+$) of the GUV. This can also be accomplished with MβCD, namely, by pre-loading it with the lipids we wish to deliver.[87] However, since our vesicles contain both phospholipids and cholesterol, and MβCD can transport both, it is advantageous to change to α-cyclodextrins: their smaller hydrophobic cavity (6 glucopyranoside units instead of 7) is too narrow to fit cholesterol but can still host individual lipid tails. Specifically, hydroxylpropyl-α-cyclodextrin (HPαCD)[93,94] and methyl-α-cyclodextrin (MαCD)[95–97] have proven to be very suitable in exchanging phospholipid content without touching cholesterol, and MαCD has been shown to be "lipid-loadable".[95]

To simplify the discussion, we will assume that the saturation ratio r_+ on the outer leaflet of the GUV remains fixed during the lipid addition process. This can be done by loading the cyclodextrins with a ratio of *u*- and *s*-lipids that reflects r_+

Open Access Article. Published on 14 januar 2025. Downloaded on 30-01-2026 17:48:09.
This article is licensed under a Creative Commons Attribution 3.0 Unported Licence.

(possibly adjusted to account for different complexation strengths). Alternatively, we could appeal to the fact that percent-level changes in α require percent-level changes in L_+ (in fact, $\Delta L_+/L = \Delta\alpha/(1-\alpha)$), but these do generally not change the saturation ratio r_+ significantly, unless it is close to 0.

As Fig. 5 indicates, the change in abundance α has opposite effects on the leaflets. Adding phospholipids to the outer leaflet will put it under compression and hence squeeze cholesterol into the inner leaflet, which had been put under tension due to the change of α. Unlike in the cholesterol depletion scenario from Section 3.2.1, where the compositions moved into the same directions and so could potentially remain quite close to $\mathscr{T} = 0$, this is not an option when we tune α: ϕ_+ moves down while ϕ_- moves up, and so the membrane will definitely develop a net torque. While it is difficult to directly compare the magnitudes of effects driven by ϕ and α, since these two variables (albeit dimensionless) measure different things, we could compare the change in $\mathscr{T}$ under conditions that give rise to the same change in ϕ_+, as is illustrated in Fig. 5. It appears evident that such a change in abundance would perturb the torque balance more strongly. Rather loosely speaking, this might translate to the statement that ternary GUVs are easier to mechanically perturb with phospholipids than with cholesterol.

4 Computational illustrations

Many of the connections we have described so far cannot (yet) be checked experimentally, but we are convinced that the rapidly growing sophistication of experimental techniques will change this in the near future. Until then, it will be useful to employ computational techniques to not just check the theoretical picture but also identify unexpected phenomena that warrant further study.

4.1 Coarse-graining as the arena for modeling

The reality of finitely available computing time puts limits on how big a system we can simulate, and for how long. Coarse-grained (CG) simulations are a popular way to overcome this constraint: develop a force field at a lower level of resolution that strives to capture physics at longer time scales and larger length scales by summarily encoding finer-scale physics in effective interactions between CG degrees of freedom. While pragmatically expedient, we would like to add that this is also good physics: a universally intriguing property of nature is that large-scale physics almost always depends on only a small number of effective parameters, with much of the intricate finer-scale detail having been rendered irrelevant. If so, it behooves us to leave such irrelevant detail out of our models, too. Notice that if we happen to ignore too much and our model no longer works, we thereby learn a deep lesson about what constitutes relevant physics.

4.1.1 The unbearable slowness of diffusion. Simulating ternary mixtures is challenging for a number of reasons, one being statistical sampling. Curvature elastic membranes are known to sample phase space slowly: their bending mode relaxation rate is $r_\kappa = \kappa q^3/4\eta$, with q being the wave vector of the mode and η the viscosity of the embedding solvent—usually water, but we could also picture a more viscous intracellular environment.

Recall, though, that (i) in particle-based simulations we are (for better or worse) not interested in the long scales but the short ones and (ii) we will also

Open Access Article. Published on 14 januar 2025. Downloaded on 30-01-2026 17:48:09.
This article is licensed under a Creative Commons Attribution 3.0 Unported Licence.

need to sample compositional fluctuations, which relax on the diffusive scale $r_D = Dq^2$, with D being the lipid diffusion constant. Comparing q^3 *vs.* q^2 shows that diffusive modes will actually relax even slower than curvature modes at sufficiently small scales. Where is the cross-over? From $\kappa {q_\times}^3/4\eta = D{q_\times}^2$ we get $\lambda_\times = 2\pi/q_\times = \pi\kappa/2D\eta$, and using typical values $\kappa \simeq 30k_BT$, $D \simeq 5\ \mu m^2\ s^{-1}$ and $\eta = 10^{-3}$ Pa s yields $\lambda_\times \simeq 40\ \mu m$. Hence, at any computational scale that bothers to actually represent lipids, we are deeply in the regime where compositional relaxation is the bottleneck.

Since the largest wavelength at which we need to sample in a simulation is the box length L, the characteristic relaxation time is ${r_D}^{-1} = L^2/4\pi^2D$. Taking $L \simeq 50$ nm (chosen to host raft-like heterogeneities at the few tens of nanometer scale), we find ${r_D}^{-1} \simeq 13\ \mu s$. While doable at the atomistic level with modern high performance computing, this remains a serious challenge and is not a feasible means to scan parameter space.

4.1.2 The course grained model we employ. We will use a highly coarse-grained solvent-free model recently developed by us.[98] It fine-tunes some key control parameters of an earlier model,[99] which itself is based on a widely-applied CG model that, however, cannot represent some of the key physics needed once asymmetry enters the stage.[100–102] Our CG model captures the notion of saturated and unsaturated lipids that differ in their specific area and the usual order parameters, a smaller rapidly flipping species of cholesterol, stretching- and bending-elasticity, spontaneous lipid curvature, and lipid diffusion; for details, see ref. 98. Crucially, this model can represent ℓ_o/ℓ_d phase coexistence in ternary mixtures, as illustrated in Fig. 6.

4.1.3 Simulation details. The CG model has its own intrinsic length-, energy-, and time-scales: σ, ε, and τ, respectively. The length scale follows

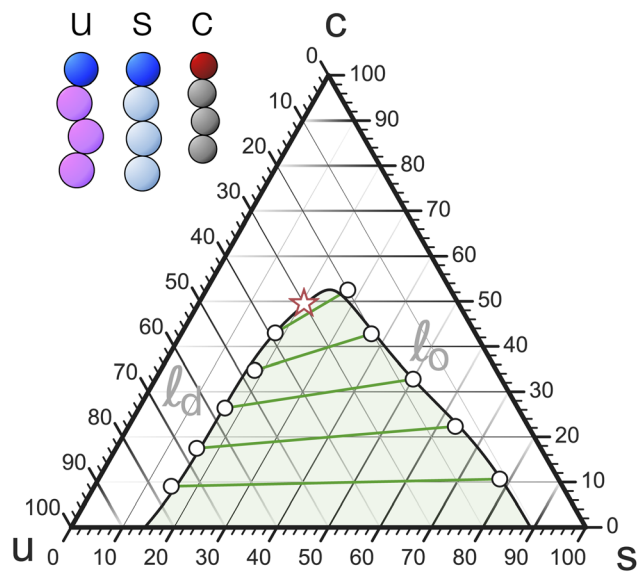

Fig. 6 Phase diagram of a ternary mixture in the Cooke lipid model of a lipid mixture, showing ℓ_o/ℓ_d coexistence and (the approximate location of) its critical point (adapted from ref. 98).

Open Access Article. Published on 14 januar 2025. Downloaded on 30-01-2026 17:48:09.
This article is licensed under a Creative Commons Attribution 3.0 Unported Licence.

straightforwardly by matching physical dimensions and leads to $\sigma \simeq 0.75$ nm. The energy scale is fixed by the temperature: we run our simulations at $k_BT = 1.4\varepsilon$, which sets ε if we assume T corresponds to the temperature at which the experiment is run, say 310 K. This finalizes the translation for various units: with $k_BT = 310\ \text{K} \times 1.38 \times 10^{-23}\ \text{J K}^{-1} = 4.28$ pN nm we get $\varepsilon = 3.06$ pN nm, $\varepsilon/\sigma = 4.08$ pN, and $\varepsilon/\sigma^2 = 5.43$ pN nm^{-1} for the units of energy, torque density, and stress (or surface tension), respectively.

The time scale is more subtle. In principle, CG degrees of freedom also have a mass m, and this defines a time scale $\tau = \tau_{\text{bare}} = \sigma\sqrt{m/\varepsilon}$, but this scale only matters for the calculation of instantaneous dynamical quantities, such as the kinetic energy. Longer time scale dynamics—diffusion, bending mode or chain relaxations, lipid flip-flop, *etc.*—is not well described by τ_{bare}, because CG models are virtually always tuned to reproduce thermodynamic equilibrium properties, not to also rescue the dynamics. In fact, the strongly sped-up dynamics resulting from a much smoother free energy landscape is a major redeeming quality of coarse-graining.

The way to translate CG dynamics into real world units is then to agree on a specific dynamical process—say, diffusion—and interpret the CG unit τ such that CG simulations of that process quantitatively map to those in the real world. For example, when a CG lipid diffusion constant is $D = 0.01\sigma^2/\tau$ (as measured for the ℓ_d phase in our model[98]) and $D = 5\ \mu\text{m}^2\ \text{s}^{-1}$ in the lab,[103] setting those equal (and recalling $\sigma = 0.75$ nm) defines $\tau \approx 1$ ns. This for instance shows that diffusive relaxation over a 50 nm $= 67\sigma$ scale happens over the time scale $11\,000\tau$, which in our case takes about 20 h on a 32 core node.

We ran our simulations using the ESPResSo package,[104] using an integration time step $\delta t = 0.005\tau$. We reach the canonical ensemble *via* a standard Langevin thermostat,[105] with a friction constant $\gamma = 1m/\tau$. To realize membranes under zero lateral tension we employed semi-anisotropic boundary conditions using a barostat of Kolb/Dünweg[106] type with a box mass $Q = 0.01m/\sigma^4$ and a friction constant $\gamma_Q = 2 \times 10^{-4} m/\sigma^4$. Our simulations typically contained 2048 lipids and ran between $80\,000\tau$ and $100\,000\tau$, with the first $20\,000\tau$ being used for thermalization.

4.2 Coexisting leaflets at very different saturation ratios

We will start by exploring coexisting leaflets that differ markedly in their saturation ratio, which creates sizable driving forces for cholesterol from one into the other. Specifically, we picked

$$r_- = 1/8 = 0.125, \tag{18a}$$

$$r_+ = 5/6 \approx 0.833. \tag{18b}$$

The low-saturation r_- line in leaf$_-$ bypasses the coexistence region, while the more ordered high-saturation r_+ line in leaf$_+$ stays outside it for $\phi \gtrsim 20\%$. Given how far the coexistence region reaches on the *s*-side for low cholesterol content, it is difficult to entirely avoid it, unless we move very close to the triangle's *sc*-side, which might bring us uncomfortably close to some not fully resolved gel complications[98] in the *s*-corner of the diagram. Observe that with this choice, cholesterol chemically prefers to partition into leaf$_+$.

Open Access Article. Published on 14 januar 2025. Downloaded on 30-01-2026 17:48:09.
This article is licensed under a Creative Commons Attribution 3.0 Unported Licence.

4.2.1 The torque surface. We have simulated systems with $N = 2048$ lipids, picking a combination of $\{\phi, \alpha\}$ states within the range $\phi \in [0, 50\%]$ and $\alpha \in [-5\%, 5\%]$, let the systems find equilibrium during approximately $20\,000\tau$, and sampled for typically another $80\,000\tau$ during which we measured a variety of observables, in particular the cholesterol distribution and asymmetry, differential stress, and torque. We found that within this domain the torque $\mathscr{T}(\phi,\alpha)$ can be represented remarkably well by a quadratic (reduced $\chi^2 = 0.11$), so we empirically fit it to

$$\mathscr{T}(\phi,\alpha) = c_0 + c_{1,\phi}\phi + c_{1,\alpha}\alpha + c_{2,\phi\phi}\phi^2 + c_{2,\alpha\alpha}\alpha^2 + c_{2,\phi\alpha}\phi\alpha. \tag{19}$$

We will refer to this as the "torque surface".

Fig. 7 shows a contour plot of that surface. For sufficiently negative values of the abundance α, *i.e.* when leaf$_+$ becomes increasingly depleted of phospholipids, the torque is positive (*i.e.*, the membrane would want to "curl up" if not prevented by the periodic boundary conditions; see Fig. 2 for a clarification of the torque's sign). Conversely, if leaf$_+$ is sufficiently overcrowded, the torque becomes negative. In between the torque crosses zero at a location dependent on the overall cholesterol content ϕ. This zero-torque-curve describes the possible states of mechanically stable GUVs, which due to their essential flatness cannot harbor any significant torque before deforming or even tubulating.

In the absence of cholesterol, $\phi = 0$, when the abundance asymmetry vanishes as well, $\alpha = 0$, but the torque is nevertheless not zero but slightly positive. This happens because the system is still not symmetric; most notably, leaf$_+$ contains an approximately six times larger fraction of saturated lipids, which have (at least in pure phases) an approximately 25% smaller area per lipid.[98] Since for $\alpha = 0$ the number of phospholipids is the same in both leaflets, the relaxed leaflet area in leaf$_+$ is smaller than in leaf$_-$, giving rise to a positive differential stress, whose torque contribution $\mathscr{T}_\Sigma = z_0 \Delta\Sigma$ wants to bend the bilayer up (see Fig. 2b).

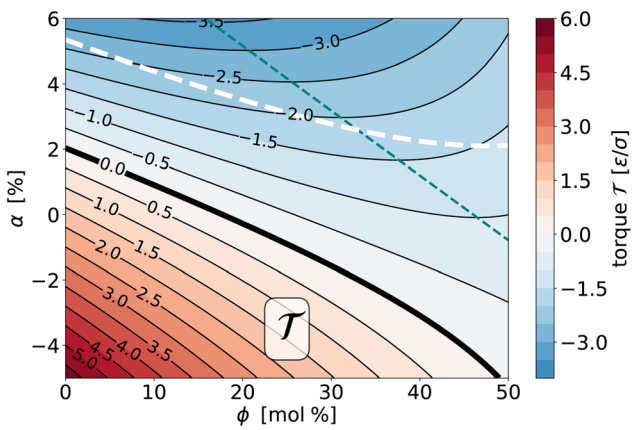

Fig. 7 Contour plot of the (empirically fitted) torque surface $\mathscr{T}(\phi,\alpha)$ for the saturation ratios $r_- = 0.125$ and $r_+ = 0.833$. The bold solid curve is the location where the torque vanishes and hence GUVs would be mechanically stable, the thin teal dashed curve is the nullcline at which $\partial\mathscr{T}/\partial\phi = \chi^{\mathscr{T}}_{\phi|\alpha} = 0$, *i.e.*, where the torque does not change upon small variations of overall cholesterol content. The bold white dashed curve is the locus of states for which $\Delta\Sigma = 0$ (see also Fig. 10).

Open Access Article. Published on 14 januar 2025. Downloaded on 30-01-2026 17:48:09.
This article is licensed under a Creative Commons Attribution 3.0 Unported Licence.

Adding cholesterol to this state will preferentially recruit it into leaf$_+$ to release the area strain, an effect that will become even stronger when we lower α. Independent of these mechanical considerations, the higher saturation ratio r_+ in leaf$_+$ will also favor the partitioning of cholesterol into it. Hence, there are two reasons that favor ϕ_+ growing faster than ϕ_-, and as a consequence, the torque decreases. Notice, though, that as we increase the abundance asymmetry α, the stress-derived torque $\mathscr{T}_\Sigma$ weakens and at some point reverses, as leaf$_-$ becomes depleted. Where will the cholesterol go, now that the two drivers compete? As the contour lines in Fig. 7 show, the trend is indeed non-monotonic: initially, $\mathscr{T}$ still decreases, since chemical partitioning bias still drives more cholesterol into leaf$_+$. But at some point it reverses, as the increasing ϕ_+ value weakens further recruitment of even more cholesterol and entropy favors a more even distribution, which together ends up reducing the magnitude of the torque. The teal dashed line in Fig. 7 marks the location of that reversal: at it, the contour lines are horizontal and $\chi^{\mathscr{T}}_{\phi|\alpha} = 0$ (which is exactly the nullcline of $\nabla\mathscr{T}$ for the variable α).

4.2.2 The response function $\chi^{\mathscr{T}}_{\phi|\alpha}$. If we cut the torque surface at some fixed value of α, we can single out the dependence of torque on ϕ: $\mathscr{T}(\phi|\alpha)$. The derivative of this function with respect to ϕ is exactly the susceptibility $\chi^{\mathscr{T}}_{\phi|\alpha}$ defined in eqn (13d), which measures how the torque changes with cholesterol content at a fixed value of α. This response function is shown in Fig. 8—itself as a function of ϕ and parametrized for a set of α-values. Due to our simple quadratic representation (19) of $\mathscr{T}(\phi,\alpha)$, we find simple lines. For most of the values the response function is negative, showing that addition of cholesterol tends to reduce the torque. However, this reduction weakens as cholesterol increases, and the $\chi^{\mathscr{T}}_{\phi|\alpha}(\phi)$ lines cross zero and become positive. This happens earlier when the abundance asymmetry is already larger. These zero crossings reflect the "trend reversal" we discussed in the previous section, *i.e.*, the nullcline included in Fig. 7.

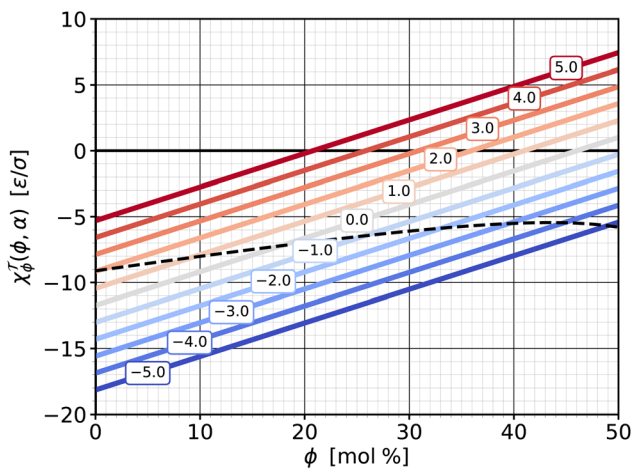

Fig. 8 Susceptibility $\chi^{\mathscr{T}}_{\phi|\alpha}$ from eqn (13d) as a function of cholesterol content ϕ, parametrized by different values of phospholipid abundance α, as indicated in the boxed labels, and the saturation ratios from eqn (18). The dashed line shows the susceptibility for the special ϕ-dependent α values at which $\mathscr{T} = 0$ (*i.e.*, on the zero-torque contour in Fig. 7).

Open Access Article. Published on 14 januar 2025. Downloaded on 30-01-2026 17:48:09.
This article is licensed under a Creative Commons Attribution 3.0 Unported Licence.

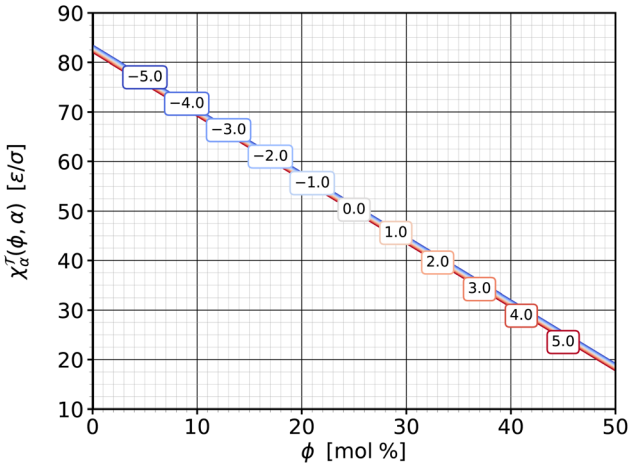

Fig. 9 Susceptibility $\chi^{\mathscr{T}}_{\alpha|\phi}$ from eqn (13b) as a function of cholesterol content ϕ, parametrized by different values of phospholipid abundance α, as indicated in the boxed labels. The lines almost coincide, with smaller α values having ever so slightly larger susceptibilities.

4.2.3 The response function $\chi^{\mathscr{T}}_{\alpha|\phi}$. We can also cut the torque surface along constant-ϕ-slices, which gives us the complementary function $\mathscr{T}(\alpha|\phi)$, whose derivative with respect to α leads to the other torque-related response function, $\chi^{\mathscr{T}}_{\alpha|\phi}$ from eqn (13b). This susceptibility—again as a function of ϕ and for a set of different α is shown in Fig. 9.

Several observations are notable here. First, the susceptibilities hardly depend on α. This means that $\partial\chi^{\mathscr{T}}_{\alpha|\phi}/\partial\alpha = -\partial^2\mathscr{T}/\partial\alpha^2 \approx 0$: the cuts of the torque surface along constant ϕ are essentially straight lines. In Fig. 7 this can be recognized by the fact that the contour curves intersect any line with a fixed ϕ value at very evenly spaced points. These lie closer together for smaller ϕ, leading to larger slopes and higher $\chi^{\mathscr{T}}_{\alpha|\phi}$ values. Physically this means that a change $\Delta\mathscr{T}$ in membrane torque due to a change $\Delta\alpha$ in phospholipid abundance does not depend on the pre-existing abundance α. A change $\Delta\Delta A$ of the area excess ΔA between the two leaflets always changes the curvature in the same way—and the parallel surface theorem[107,108] agrees: $\Delta\Delta A = 2Az_0\Delta J$, provided that adding or removing phospholipids always adds or removes the same area.

Second, the susceptibility $\chi^{\mathscr{T}}_{\alpha|\phi}$ is positive. The definite sign (unlike what we have seen for the complementary partner $\chi^{\mathscr{T}}_{\phi|\alpha}$) derives from the expectation that adding phospholipids on one side invariably bends the membrane away from that side. Since adding lipids to leaf$_+$ increases α, but a downward bending counts as a negative torque (*cf.* again Fig. 2), we have added an additional minus sign to the definition (13b) of $\chi^{\mathscr{T}}_{\alpha|\phi}$ to arrange for a convenient positive sign. This mimics definitions such as $\kappa_T = -(\partial V/\partial P)_T/V$ for the isothermal compressibility (whose sign is fixed by a rigorous thermodynamic argument, though, not merely a strong expectation).

Third, the magnitude of $\chi^{\mathscr{T}}_{\alpha|\phi}$ is noticeably larger than that of $\chi^{\mathscr{T}}_{\phi|\alpha}$. Small changes of the phospholipid abundance α change the torque more strongly than comparably small changes of the cholesterol content ϕ. As mentioned above, the reason is

Open Access Article. Published on 14 januar 2025. Downloaded on 30-01-2026 17:48:09.
This article is licensed under a Creative Commons Attribution 3.0 Unported Licence.

that changes in α have a sign built into it: all phospholipids are added or removed from the same leaflet, while cholesterol addition or removal is shared between the two leaflets (besides the fact that cholesterol molecules are also smaller).

4.2.4 The differential stress surface. Just as we can measure the torque $\mathscr{T}$ as a function of the two thermodynamic variables ϕ and α, we can do the same with the differential stress $\Delta\Sigma$. The procedure mirrors the one for the torque surface from Section 4.2.1; in particular, we again find that a quadratic fit captures the simulated data very well. Fig. 10 shows the result *via* a contour plot, amended again by the nullcline at which $\partial\Delta\Sigma/\partial\phi = \chi^{\Delta\Sigma}_{\phi|\alpha} = 0$, a bold contour curve to highlight the place where the differential stress vanishes, and for comparison also the location of the curve where the torque vanishes. Let us summarize several notable points:

(1) As we deplete phospholipids from leaf$_+$ (*i.e.*, reduce α), the differential stress increases.

(2) The variation with ϕ is again a bit more subtle, since for sufficiently large α an initial reduction in $\Delta\Sigma$, driven by preferential partitioning, can reverse direction for sufficiently large ϕ, when stress and entropy take over.

(3) Torque and differential stress never vanish at the same time: zero torque states have a positive differential stress, while zero differential stress states have a negative torque.

(4) The $\mathscr{T} = 0$ curve lies very close to the $\Delta\Sigma = 1.0\varepsilon/\sigma^2$ contour line, which shows that all possible zero torque states have (within about $\pm 7\%$) the same differential stress.

(5) Just as for the torque, we could also plot the two susceptibilities $\chi^{\Delta\Sigma}_{\phi|\alpha}$ and $\chi^{\Delta\Sigma}_{\alpha|\phi}$, but they behave qualitatively very similarly to their torque counterparts. Briefly, the $\chi^{\Delta\Sigma}_{\phi|\alpha}$ are lines with positive slope that at the nullcline transition from negative to positive values, and this happens earlier for larger α. The $\chi^{\Delta\Sigma}_{\alpha|\phi}$ are

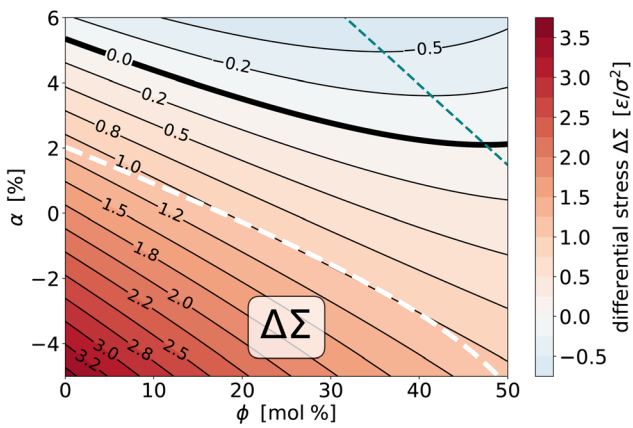

Fig. 10 Contour plot of the (empirically fitted) differential stress surface $\Delta\Sigma(\phi, \alpha)$ for the saturation ratios $r_- = 0.125$ and $r_+ = 0.833$. The bold solid curve is the location where the differential stress vanishes, the thin teal dashed curve is the nullcline at which $\partial\Delta\Sigma/\partial\phi = \chi^{\Delta\Sigma}_{\phi|\alpha} = 0$, *i.e.*, where the differential stress does not change upon small variations of overall cholesterol content. The bold white dashed curve is the locus of states for which $\mathscr{T} = 0$ (see also Fig. 7).

Open Access Article. Published on 14 januar 2025. Downloaded on 30-01-2026 17:48:09.
This article is licensed under a Creative Commons Attribution 3.0 Unported Licence.

positive, generally larger in magnitude, decreasing with ϕ, and again hardly dependent on α.

4.2.5 Leaflet spontaneous curvature and its torque. Let us specialize eqn (5b), which links torque and stress, to a flat state—as relevant to our simulations:

$$\kappa J_{0,\mathrm{b}} = z_0 \Delta\Sigma - \mathscr{T} \text{ (flat membrane).} \tag{20}$$

Since we now have both the torque and the differential stress surface available, we can obtain the lipid-shape affiliated spontaneous bilayer curvature torque $\kappa J_{0,\mathrm{b}}$ for a wide range of conditions, assuming we know z_0. Taking $z_0 \simeq 2\sigma$ for our model, we find that $\kappa J_{0,\mathrm{b}}$ varies fairly little over the explored parameter range (mostly between $1.5\varepsilon/\sigma$ and $2.5\varepsilon/\sigma$). This is surprising, since we would expect that changing cholesterol content or compressing/stretching a leaflet affects the conformational ensemble of lipids, and hence their preferred curvature. Clearly, the extent to which this happens will also depend on details of the lipid model, and this question should be revisited with different models, especially those at a more refined resolution.

Let us map this finding to realistic units: recalling that $\sigma \approx 0.75$ nm and $k_{\mathrm{B}}T = 1.4\varepsilon$, we find $z_0 \approx 1.5$ nm and $\kappa J_{0,\mathrm{b}} \approx 2\varepsilon/\sigma \approx 1.9 k_{\mathrm{B}}T$/nm. If we recall that the bending rigidity of our CG membranes is around $\kappa \approx 30 k_{\mathrm{B}}T$,[99] which is similar to real lipid membranes, the lipid torque translates to a spontaneous bilayer curvature of $J_{0,\mathrm{b}} \approx 0.063\ \mathrm{nm}^{-1}$. This corresponds to an equilibrium vesicle radius $R_0 = 2/J_{0,\mathrm{b}} \approx 32$ nm, in line with the typical expectations we have outlined in Section 3.1. This reiterates that unless differential stress cancels the torque associated with lipid shape, these systems cannot exist as stable GUVs. But it also shows that our fairly simple CG model reproduces the orders of magnitude of some of these effects quite well.

4.2.6 Tentative application to biological systems. The exoplasmic leaflet of cell membranes is significantly more saturated than the cytosolic one; for instance, Lorent *et al.*[50] show that cytosolic phospholipids in the human red blood cell membrane have about twice as many double bonds as their exoplasmic counterparts. Their data and models also suggest $r_+/r_- \approx 5.5$—not too far off from our current example $r_- = 0.125$ and $r_+ = 0.833$, which yields the slightly larger contrast $r_+/r_- \approx 6.7$. Let us hence take these saturation ratios as a crude proxy for a plasma membrane (with leaf$_+$ being the outer one) and add 40 mol% cholesterol to match the physiological situation. What type of membrane do we get, if we insist on an overall torque-free state?

From Fig. 7 we see that the zero-torque contour intersects $\phi = 40\%$ at a phospholipid abundance of $\alpha \approx -3.1\%$. Explicit simulations at this state point confirm that the torque vanishes within error ($\mathscr{T} = 0.12(12)\varepsilon/\sigma$) but the differential stress does not: $\Delta\Sigma = 1.01(06)\varepsilon/\sigma^2$, in agreement with Fig. 10. The cytosolic leaflet hence contains more phospholipids than the exoplasmic one, an abundance asymmetry partially balanced by cholesterol: we find $\phi_+ = 45\%$ and $\phi_- = 34\%$, showing that about 57% of all cholesterol is in leaf$_+$.

That the exoplasmic leaflet contains fewer phospholipids is a subtle balance between several competing factors: at first one might think that a leaflet richer in more saturated lipids, which have a smaller specific area, should contain more of those lipids. This is indeed true when we remove all cholesterol: as we have seen, the zero-torque contour intersects $\phi = 0\%$ at $\alpha \simeq 2\%$, *i.e.*, at a slightly positive

Open Access Article. Published on 14 januar 2025. Downloaded on 30-01-2026 17:48:09.
This article is licensed under a Creative Commons Attribution 3.0 Unported Licence.

phospholipid abundance. But we have two competing effects: first, the excess of saturated lipids in the outer leaflet renders $J_{0,b}$ slightly positive. This creates a negative bilayer torque $\mathscr{T}_\kappa$ which we must "undo" by a positive differential stress to stay at $\mathscr{T} = 0$ (see eqn (5b)); this favors reducing the phospholipid contingent in leaf$_+$ even in the absence of cholesterol. And second, the saturated lipids in the outer leaflet recruit cholesterol more avidly. As we increase ϕ, the cholesterol mole fraction ϕ_+ will hence grow more strongly than ϕ_-.

Taking everything together, the initial exoplasmic abundance "flips" beyond $\phi \approx 18\%$: torque-free membranes now have more phospholipids in their cytosolic leaflet. This is qualitatively in line with experimental observations, but the quantitative comparison is far off: in our case, at 40% cholesterol the cytosolic leaflet contains about 6% more phospholipids than the exoplasmic one, while recent experiments argue that the excess can be 100% or even more—a factor of 2.[76] Of course, we must be careful with predictions based on coarse-grained models as simplified as ours: while we have tried to capture many important characteristics of this system when we developed our force-field (such as lipid area, cholesterol partitioning, and the overall phase behavior),[98] more subtle phenomena (*e.g.*, how does lipid spontaneous curvature depend on saturation and cholesterol content) need to be further examined. That being said, this large discrepancy serves to remind us how extraordinary the experimental claims are, and how difficult it would be to achieve a torque balanced state with an acceptable differential stress at a much larger abundance asymmetry (assuming, of course, that torque balance is relevant to begin with).

4.3 Demixing driven by differential stress

As a final illustration we show how a system of fixed overall lipid content can be driven to phase segregate in one leaflet by depleting its cholesterol content *via* a suitably induced differential stress.

4.3.1 System setup. For equilibration reasons it is easier to create ℓ_o domains in an ℓ_d background, and so we will pick the ℓ_d-leaflet (which for consistency we make leaf$_-$) to be the one to phase separate. Specifically, let us pick a saturation ratio $r_- = 0.2$, which results in a line that intersects the ℓ_o/ℓ_d coexistence region in the vicinity of $\phi_- = 20\%$ (see Fig. 11). To keep matters simple, we will choose the composition in leaf$_+$ to be as far away from coexistence as possible, namely, on the binary *sc*-side of the triangle (*i.e.*, at $r_+ = 1$).

With this choice of $r_\pm$, we ran a set of simulations at $\alpha = 0$ over a range of overall cholesterol concentrations $\phi \in \{10\%, 15\%, 20\%, \ldots, 50\%\}$ and let these relax until both sides found their equilibrium cholesterol content $\phi_\pm$. The purpose is to find the ϕ-value that lets ϕ_- sit as close as possible to the binodal of the coexistence region, so that subsequent changes in differential stress, which raise or lower ϕ_-, will move leaf$_-$ further away or more deeply into the coexistence region.

Since the specific area of *s*-lipids is about 25% smaller than that of *u*-lipids, we expect a system with the same number of phospholipids on both sides (*i.e.*, $\alpha = 0$) to be under negative differential stress (*i.e.*, leaf$_+$ is under tension while leaf$_-$ is compressed). The presumably cleanest way to run the simulations is to compensate for this and increase the abundance until $\Delta\Sigma = 0$. This is technically challenging, though, since the necessary increase is itself ϕ-dependent (recall the

Open Access Article. Published on 14 januar 2025. Downloaded on 30-01-2026 17:48:09.
This article is licensed under a Creative Commons Attribution 3.0 Unported Licence.

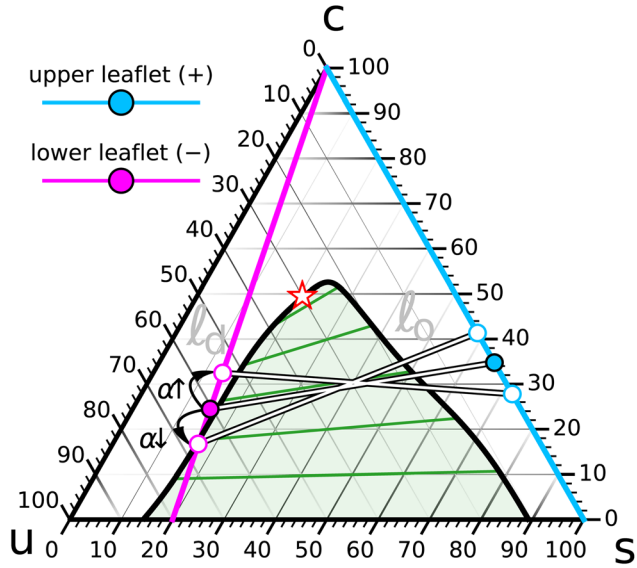

Fig. 11 The set of saturation ratios $r_+ = 1$ for leaf$_+$ (cyan line) and $r_- = 0.2$ for leaf$_-$ (magenta line), combined with an overall cholesterol content $\phi = 30\%$, yields a pair of coexisting points (solid cyan and magenta symbols) of which the leaf$_-$ composition resides very close to the ℓ_d-side of the binodal. Increasing the abundance asymmetry $\alpha \to +10\%$ squeezes cholesterol from leaf$_+$ to leaf$_-$ and pushes the latter further away from the two phase region. Reducing $\alpha \to -10\%$ instead removes cholesterol from leaf$_-$ and plunges it into ℓ_o/ℓ_d coexistence (see Fig. 12 for illustrations). The compositions in leaf$_+$ pivot oppositely but always stay in a homogeneous ℓ_o phase.

nontrivial ϕ–α relation on the $\Delta\Sigma = 0$ contour of the differential stress surface shown in Fig. 10). To avoid an extra round of iterations, we decided to forgo this ambition and instead select an overall cholesterol content ϕ that results in a ϕ_- slightly above the coexistence region, as we expect the slight net compression in leaf$_-$ to assist the formation of ordered domains. With this in mind, we selected $\phi = 30\%$, which resulted in $\phi_- \approx 24.5\%$, about 5 percentage points above the local cholesterol content of the binodal. Fortuitously, the resulting system has an almost vanishing torque, $\mathscr{T} = -0.33(17)\varepsilon/\sigma \simeq -1.3(7)$ pN, meaning, it would be voluntarily (close to) flat.

Observe that the r_- line and the binodal intersect at a relatively small angle, such that small movements of the binodal to the left or right would shift the intersection by a fairly large amount. The binodal is indeed not known very precisely, as its location is not merely dependent on sampling (slow) statistical fluctuations in the compositions of coexisting ℓ_o/ℓ_d phases (see ref. 98 for details) but also on difficult to quantify systematic errors inherent in the Hidden Markov Model's phase identification.[98,109] With these complications in mind, we chose to not over-engineer the precise location of ϕ_-.

4.3.2 Driving the leaflet into the coexistence region. While the chosen system with $\phi = 30\%$ has leaf$_-$ close to the ℓ_d-side of the binodal, leaf$_+$ is far from coexistence and manifestly in a homogeneous ℓ_o phase at $r_+ = 1$ and $\phi_+ = 34.8\%$, see again the phase diagram in Fig. 11. We now create two new systems in which

Open Access Article. Published on 14 januar 2025. Downloaded on 30-01-2026 17:48:09.
This article is licensed under a Creative Commons Attribution 3.0 Unported Licence.

we change the abundance asymmetry to $\alpha = +10\%$ and $\alpha = -10\%$. The former increases the number of phospholipids in leaf$_+$ relative to leaf$_-$ and hence expels some of the cholesterol into leaf$_-$, where its concentration increases to about $\phi_- = 32.5\%$, moving it further away from the binodal. In the other case we instead deplete leaf$_+$ relative to leaf$_-$ and thus draw additional cholesterol from leaf$_-$, where its concentration hence drops even more, to about $\phi_- = 16.7\%$, thereby plunging this leaflet into the coexistence region.

Fig. 12 shows stylized snapshots of the leaf$_-$ lipid configuration for the three systems with $\alpha \in \{-10\%, 0\%, +10\%\}$. As the abundance changes from negative to positive, and as a consequence the leaflet's cholesterol content from a small to a larger value, we observe that very distinct stable ℓ_o domains visible at $\alpha = -10\%$ melt away, with merely some remnant transient non-ideally mixed "flakes" remaining, which dynamically fluctuate in and out of existence.

4.3.3 Associated mechanical variables. The differential stress driving cholesterol translocation is quite substantial: as the values in Fig. 12 show, $\Delta\Sigma$ changes by almost 25 pN nm^{-1}, while the torque changes by about 37 pN. Since these changes appear linear with abundance, we get simple estimates for the α-driven susceptibilities:

$$\chi^{\Delta\Sigma}_{\alpha|\phi} \approx -\frac{\Delta\Delta\Sigma}{\Delta\alpha} \approx 23\varepsilon/\sigma^2 \simeq 124 \text{ pN nm}^{-1}, \tag{21a}$$

$$\chi^{\mathscr{T}}_{\alpha|\phi} \approx -\frac{\Delta\mathscr{T}}{\Delta\alpha} \approx 46\varepsilon/\sigma \simeq 187 \text{ pN}. \tag{21b}$$

Interestingly, the value for $\chi^{\mathscr{T}}_{\alpha|\phi}$ is essentially the same we found in Section 4.2.3 (see Fig. 9 at $\phi = 30\%$), even though the $r_\pm$ values were different. This suggests that the response to a change in lipid abundance is dominated by mechanics. We

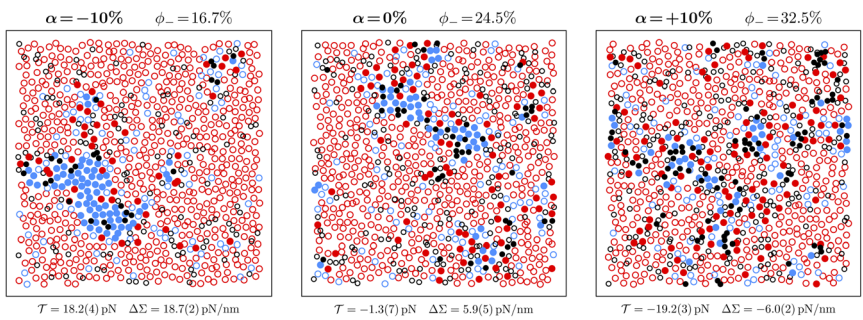

Fig. 12 Stylized representative lipid configurations in leaf$_-$ of the three systems discussed in Section 4.3 and represented in the phase diagram of Fig. 11. Colors indicate lipid type—red: unsaturated, blue: saturated, black: cholesterol—while style indicates the phase state—open circles: ℓ_d, filled circles: ℓ_o—as identified by a Hidden Markov Model analysis.[98,109] At zero abundance, the phase state in leaf$_-$ is very close to the ℓ_d-side of the coexistence binodal and we see only fleeting occurrences of small transient ℓ_o regions. At $\alpha = -10\%$ cholesterol is drawn out of leaf$_-$ which pushes the phase state into the coexistence region and we get a small but persistent ℓ_o domain. Conversely, at $\alpha = +10\%$ cholesterol is pushed from leaf$_+$ into leaf$_-$, increasing the state's distance from the coexistence region and further melting any remaining ordered domains. All systems contain 2048 lipids, and the box length is approximately $L \approx 32\sigma \approx 24$ nm.

Open Access Article. Published on 14 januar 2025. Downloaded on 30-01-2026 17:48:09.
This article is licensed under a Creative Commons Attribution 3.0 Unported Licence.

already saw that $\chi^{\mathscr{T}}_{\alpha|\phi}$ itself hardly depends on α; here we get additional support from the fact that the change in torque is almost exclusively driven by the change in differential stress.

Using eqn (20) to calculate the intrinsic torque $\kappa J_{0,\mathrm{b}}$, and taking again $z_0 = 2\sigma \simeq 1.5$ nm, we find that $\kappa J_{0,\mathrm{b}} \simeq 10$ pN within error for all three systems. The value itself is quite reasonable (using again $\kappa \approx 30 k_{\mathrm{B}}T$ we get $J_{0,\mathrm{b}} \simeq 0.08\ \mathrm{nm}^{-1}$), but its ϕ-independence appears surprising, given that the $\alpha = +10\%$ system has about twice as much cholesterol in leaf$_-$ as the $\alpha = -10\%$ system, with a slightly smaller but opposite effect in leaf$_+$, and so we would expect some effect at the spontaneous curvature level. Of course, the precise answer depends on exactly what value we use for z_0, and that value itself can change as leaflets become more or less ordered and hence lipids stretch or shrink. Furthermore, the mechanism by which cholesterol affects intrinsic lipid curvature is notoriously subtle,[78,80] and we should not expect this to be fully captured by a coarse-grained model as simple as ours.

The magnitude of these stresses and torques raises concerns about whether under experimental conditions these systems would remain stable. Unbalanced torques of order 18 pN may be associated with characteristic curvature radii $R \sim 2\kappa/\mathscr{T} \sim 14$ nm. Our box length $L \approx 24$ nm is not much larger than this, and so curvature deformations such as tubulation are not an option, but they would be for macroscopic systems at the micron scale. To still observe a single leaflet phase transition we have to relocate enough cholesterol with less stress. We suspect the experimental situation is easier, though, as we will not need to change a leaflet's cholesterol content by as much as 15% to affect a very noticeable difference in its phase state. Macroscopic systems respond much more sharply when crossing first order phase boundaries. However, considering that transitions from nanoscopic domains to macroscopic phase separation appear to be another characteristic of these systems,[110–112] we must be careful not to over-interpret findings obtained from small simulations.

Conclusions

We have proposed a thermodynamic framework that describes the conditions for coexistence between the two leaflets of an asymmetric ternary lipid membrane comprising a saturated lipid, an unsaturated lipid, and cholesterol. Our goal was not to make specific predictions—the discussion remains fully agnostic about the detailed form of the system's free energy. Instead, we clarified the dimensionality of the underlying thermodynamic state space, arguing that even though cholesterol will transition between leaflets to equilibrate its chemical potential, two essentially arbitrary ternary compositions can still coexist. However, doing so will generally require a nonzero differential stress $\Delta\Sigma$ that creates a mechanical counter-pressure to act against a generally non-zero chemical driving force. This implies that $\Delta\Sigma$ is an essential thermodynamic variable that must be part of any description of the asymmetric ternary system, for otherwise not the entire available state space is also accessible.

Differential stress not only helps achieve a certain desired cholesterol imbalance; since individual leaflet tensions act some distances $\pm z_0$ displaced from the membrane midplane, $\Delta\Sigma$ creates a torque. This torque, in turn, will combine with the generally nonzero intrinsic torque due to lipid compositional asymmetry into an overall torque $\mathscr{T}$ that will try to bend the membrane. We argue that large

Open Access Article. Published on 14 januar 2025. Downloaded on 30-01-2026 17:48:09.
This article is licensed under a Creative Commons Attribution 3.0 Unported Licence.

membranes such as GUVs are therefore only stable against small-scale tubulation if the overall torque indeed vanishes.

Keeping track of the accessible degrees of freedom is hence rather subtle: two two-dimensional composition spaces (*i.e.*, two Gibbs triangles per leaflet) combine to 4 degrees of freedom, but the equilibrium condition $\mu_{\mathrm{chol}}{}^{+} = \mu_{\mathrm{chol}}{}^{-}$ removes one, leaving only 3. However, differential stress can help balance cholesterol, so including it we bounce back to 4. Except, if the resulting torque is not also close to zero, the membrane is unstable against tubulation, so we again drop down to 3.

All these complications can be traced back to cholesterol, a remarkable actor that plays two entirely different roles here: on the one hand it co-determines the phase behavior as one of the compositional axes in the Gibbs triangles. On the other hand it can transition between leaflets and hence change the inter-leaflet stresses. Recall now that cholesterol also affects the intrinsic curvature of mixtures, usually not additively, and that its effect on leaflet area is not just non-additive but maybe also non-positive (because under certain conditions adding cholesterol will condense the membrane). This shows that writing down an actual free energy, or equations of state, for these coexisting asymmetric ternary systems is going to be a significant challenge, which we probably have to approach by adding complications one step at a time. This was not the goal of this paper, but we hope that the conceptual framework we have provided here will make it easier to progress on this difficult journey.

Data availability

The code used to set up the simulations, along with various data analysis scripts used in this article, are available on GitHub: **https://github.com/m-varma-phys/asymmetric_ternary_mixtures**.

Author contributions

Malavika Varma: conceptualization (supporting); formal analysis (lead); investigation (equal); methodology (lead); software (lead); visualization (supporting); writing—review & editing (equal). Markus Deserno: conceptualization (lead); investigation (equal); funding acquisition (lead); visualization (lead); project administration (lead); supervision (lead); writing—original draft (lead); writing—review & editing (equal).

Conflicts of interest

There are no conflicts to declare.

Acknowledgements

The authors are grateful for many stimulating discussions on the subject with Ilya Levental, Kandice Levental, Sarah Veatch, Milka Doktorova, Fred Heberle, Thais Enoki, Alex Sodt, Gerald Feigenson, Samuel Foley, Seamus Gallagher, and Tyler Reagle. This material is based upon work supported by the National Science Foundation under Award No. NSF/CHE 2102316.

Open Access Article. Published on 14 januar 2025. Downloaded on 30-01-2026 17:48:09.
This article is licensed under a Creative Commons Attribution 3.0 Unported Licence.

Notes and references

1 G. van Meer, *EMBO J.*, 2005, **24**, 3159–3165.
2 M. R. Wenk, *Nat. Rev. Drug Discovery*, 2005, **4**, 594–610.
3 G. van Meer, *Annu. Rev. Cell Biol.*, 1989, **5**, 247–275.
4 J. E. Kyle, L. Aimo, A. J. Bridge, G. Clair, M. Fedorova, J. B. Helms, M. R. Molenaar, Z. Ni, M. Orešič, D. Slenter, E. Willighagen and B.-J. M. Webb-Robertson, *Metabolomics*, 2021, **17**, 55.
5 K. Simons and E. Ikonen, *Nature*, 1997, **387**, 569–572.
6 D. A. Brown and E. London, *Annu. Rev. Cell Dev. Biol.*, 1998, **14**, 111–136.
7 D. A. Brown and E. London, *J. Biol. Chem.*, 2000, **275**, 17221–17224.
8 K. Simons and D. Toomre, *Nat. Rev. Mol. Cell Biol.*, 2000, **1**, 31–39.
9 K. Simons and M. J. Gerl, *Nat. Rev. Mol. Cell Biol.*, 2010, **11**, 688.
10 L. J. Pike, *J. Lipid Res.*, 2006, **47**, 1597–1598.
11 S. Munro, *Cell*, 2003, **115**, 377–388.
12 I. Levental and S. L. Veatch, *J. Mol. Biol.*, 2016, **428**, 4749–4764.
13 F. M. Goñi, *Chem. Phys. Lipids*, 2019, **218**, 34–39.
14 I. Levental, K. R. Levental and F. A. Heberle, *Trends Cell Biol.*, 2020, **30**, 341–353.
15 G. W. Feigenson and J. T. Buboltz, *Biophys. J.*, 2001, **80**, 2775–2788.
16 S. L. Veatch and S. L. Keller, *Phys. Rev. Lett.*, 2002, **89**, 268101.
17 S. L. Veatch and S. L. Keller, *Biophys. J.*, 2003, **85**, 3074–3083.
18 D. Scherfeld, N. Kahya and P. Schwille, *Biophys. J.*, 2003, **85**, 3758–3768.
19 S. L. Veatch, I. V. Polozov, K. Gawrisch and S. L. Keller, *Biophys. J.*, 2004, **86**, 2910–2922.
20 S. L. Veatch and S. L. Keller, *Biochim. Biophys. Acta, Biomembr.*, 2005, **1746**, 172–185.
21 S. L. Veatch and S. L. Keller, *Phys. Rev. Lett.*, 2005, **94**, 148101.
22 H. McConnell, *Biophys. J.*, 2005, **88**, L23–L25.
23 S. L. Veatch, K. Gawrisch and S. L. Keller, *Biophys. J.*, 2006, **90**, 4428–4436.
24 G. W. Feigenson, *Annu. Rev. Biophys. Biomol. Struct.*, 2007, **36**, 63–77.
25 T. Baumgart, G. Hunt, E. R. Farkas, W. W. Webb and G. W. Feigenson, *Biochim. Biophys. Acta, Biomembr.*, 2007, **1768**, 2182–2194.
26 A. Bunge, P. Müller, M. Stöckl, A. Herrmann and D. Huster, *Biophys. J.*, 2008, **94**, 2680–2690.
27 D. Marsh, *Biochim. Biophys. Acta, Biomembr.*, 2009, **1788**, 2114–2123.
28 Y. Z. Yoon, J. P. Hale, P. G. Petrov and P. Cicuta, *J. Phys.: Condens. Matter*, 2010, **22**, 062101.
29 F. A. Heberle, J. Wu, S. L. Goh, R. S. Petruzielo and G. W. Feigenson, *Biophys. J.*, 2010, **99**, 3309–3318.
30 F. A. Heberle and G. W. Feigenson, *Cold Spring Harbor Perspect. Biol.*, 2011, **3**, a004630.
31 M. C. Blosser, J. B. Starr, C. W. Turtle, J. Ashcraft and S. L. Keller, *Biophys. J.*, 2013, **104**, 2629–2638.
32 S. L. Veatch, O. Soubias, S. L. Keller and K. Gawrisch, *Proc. Natl. Acad. Sci. U. S. A.*, 2007, **104**, 17650–17655.
33 A. R. Honerkamp-Smith, P. Cicuta, M. D. Collins, S. L. Veatch, M. Den Nijs, M. Schick and S. L. Keller, *Biophys. J.*, 2008, **95**, 236–246.

Open Access Article. Published on 14 januar 2025. Downloaded on 30-01-2026 17:48:09.
This article is licensed under a Creative Commons Attribution 3.0 Unported Licence.

34 A. R. Honerkamp-Smith, S. L. Veatch and S. L. Keller, *Biochim. Biophys. Acta, Biomembr.*, 2009, **1788**, 53–63.
35 L. S. Hirst, P. Uppamoochikkal and C. Lor, *Liq. Cryst.*, 2011, **38**, 1735–1747.
36 S. L. Veatch and P. Cicuta, *Physics of Biological Membranes*, Springer, 2018, pp. 141–168.
37 E. Cammarota, C. Soriani, R. Taub, F. Morgan, J. Sakai, S. L. Veatch, C. E. Bryant and P. Cicuta, *J. R. Soc. Interface*, 2020, **17**, 20190803.
38 T. R. Shaw, S. Ghosh and S. L. Veatch, *Annu. Rev. Phys. Chem.*, 2021, **72**, 51–72.
39 S. L. Veatch, P. Cicuta, P. Sengupta, A. Honerkamp-Smith, D. Holowka and B. Baird, *ACS Chem. Biol.*, 2008, **3**, 287–293.
40 J. Huang, J. T. Buboltz and G. W. Feigenson, *Biochim. Biophys. Acta, Biomembr.*, 1999, **1417**, 89–100.
41 J. Huang and G. W. Feigenson, *Biophys. J.*, 1999, **76**, 2142–2157.
42 M. S. Bretscher, *Nature (London), New Biol.*, 1972, **236**, 11.
43 S. J. Singer and G. L. Nicolson, *Science*, 1972, **175**, 720–731.
44 A. J. Verkleij, R. F. A. Zwaal, B. Roelofsen, P. Comfurius, D. Kastelijn and L. L. M. Van Deenen, *Biochim. Biophys. Acta, Biomembr.*, 1973, **323**, 178–193.
45 P. K. Schick, K. B. Kurica and G. K. Chacko, *J. Clin. Invest.*, 1976, **57**, 1221–1226.
46 A. Sandra and R. E. Pagano, *Biochemistry*, 1978, **17**, 332–338.
47 J. A. F. Op den Kamp, *Annu. Rev. Biochem.*, 1979, **48**, 47–71.
48 P. F. Devaux, *Biochemistry*, 1991, **30**, 1163–1173.
49 M. G. P. Vale, *Biochim. Biophys. Acta, Biomembr.*, 1977, **471**, 39–48.
50 J. H. Lorent, K. R. Levental, L. Ganesan, G. Rivera-Longsworth, E. Sezgin, M. Doktorova, E. Lyman and I. Levental, *Nat. Chem. Biol.*, 2020, **16**, 644–652.
51 M. M. Sperotto and A. Ferrarini, *The Biophysics of Cell Membranes: Biological Consequences*, Springer Singapore, Singapore, 2017, pp. 29–60.
52 W. F. D. Bennett, J. L. MacCallum, M. J. Hinner, S. J. Marrink and D. P. Tieleman, *J. Am. Chem. Soc.*, 2009, **131**, 12714–12720.
53 S. Jo, H. Rui, J. B. Lim, J. B. Klauda and W. Im, *J. Phys. Chem. B*, 2010, **114**, 13342–13348.
54 R.-X. Gu, S. Baoukina and D. P. Tieleman, *J. Chem. Theory Comput.*, 2019, **15**, 2064–2070.
55 R. E. Scott, *Science*, 1976, **194**, 743–745.
56 R. E. Scott and P. B. Maercklein, *J. Cell Sci.*, 1979, **35**, 245–252.
57 D. Holowka and B. Baird, *Biochemistry*, 1983, **22**, 3466–3474.
58 E. Sezgin, H.-J. Kaiser, T. Baumgart, P. Schwille, K. Simons and I. Levental, *Nat. Protoc.*, 2012, **7**, 1042–1051.
59 D. M. Engelman, *Nature*, 2005, **438**, 578–580.
60 T. Baumgart, A. T. Hammond, P. Sengupta, S. T. Hess, D. A. Holowka, B. A. Baird and W. W. Webb, *Proc. Natl. Acad. Sci. U. S. A.*, 2007, **104**, 3165–3170.
61 H. Keller, M. Lorizate and P. Schwille, *ChemPhysChem*, 2009, **10**, 2805–2812.
62 M. Krompers and H. Heerklotz, *Membranes*, 2023, **13**, 267.
63 A. Hossein and M. Deserno, *Biophys. J.*, 2020, **118**, 624–642.
64 A. Hossein and M. Deserno, *J. Chem. Phys.*, 2021, **154**, 014704.
65 S. L. Foley, A. Hossein and M. Deserno, *Biophys. J.*, 2022, **121**, 2997–3009.
66 S. L. Foley, M. Varma, A. Hossein and M. Deserno, *Emerging Top. Life Sci.*, 2023, **7**, 95–110.

Open Access Article. Published on 14 januar 2025. Downloaded on 30-01-2026 17:48:09.
This article is licensed under a Creative Commons Attribution 3.0 Unported Licence.

67 M. Deserno, *Curr. Opin. Struct. Biol.*, 2024, **87**, 102832.
68 C. E. Morris and U. Homann, *J. Membr. Biol.*, 2001, **179**, 79–102.
69 T. A. Enoki and F. A. Heberle, *Proc. Natl. Acad. Sci. U. S. A.*, 2023, **120**, e2308723120.
70 A. J. Wagner, S. Loew and S. May, *Biophys. J.*, 2007, **93**, 4268–4277.
71 G. G. Putzel and M. Schick, *Biophys. J.*, 2008, **94**, 869–877.
72 S. May, *Soft Matter*, 2009, **5**, 3148–3156.
73 J. J. Williamson and P. D. Olmsted, *Biophys. J.*, 2015, **108**, 1963–1976.
74 J. J. Williamson and P. D. Olmsted, *Soft Matter*, 2015, **11**, 8948–8959.
75 J. J. Williamson and P. D. Olmsted, *Biophys. J.*, 2018, **115**, 1956–1965.
76 M. Doktorova, J. L. Symons, X. Zhang, H.-Y. Wang, J. Schlegel, J. H. Lorent, F. A. Heberle, E. Sezgin, E. Lyman, K. R. Levental and I. Levental, *Cell*, 2025, **188**, 1–17.
77 M. Varma and M. Deserno, *Biophys. J.*, 2022, **121**, 4001–4018.
78 A. J. Sodt, R. M. Venable, E. Lyman and R. W. Pastor, *Phys. Rev. Lett.*, 2016, **117**, 138104.
79 D. W. Allender, A. J. Sodt and M. Schick, *Biophys. J.*, 2019, **116**, 2356–2366.
80 A. H. Beaven, K. Sapp and A. J. Sodt, *Biophys. J.*, 2023, **122**, 2162–2175.
81 R. M. Venable, F. L. Brown and R. W. Pastor, *Chem. Phys. Lipids*, 2015, **192**, 60–74.
82 U. Seifert, K. Berndl and R. Lipowsky, *Phys. Rev. A: At., Mol., Opt. Phys.*, 1991, **44**, 1182–1202.
83 U. Seifert, *Adv. Phys.*, 1997, **46**, 13–137.
84 R. Lipowsky, *Faraday Discuss.*, 2013, **161**, 305–331.
85 Y. Liu, J. Agudo-Canalejo, A. Grafmüller, R. Dimova and R. Lipowsky, *ACS Nano*, 2016, **10**, 463–474.
86 R. Lipowsky, *Adv. Biol.*, 2022, **6**, 2101020.
87 T. Reagle, Y. Xie, Z. Li, W. Carnero and T. Baumgart, *Soft Matter*, 2024, **20**, 4291–4307.
88 R. Zidovetzki and I. Levitan, *Biochim. Biophys. Acta, Biomembr.*, 2007, **1768**, 1311–1324.
89 S. Mahammad and I. Parmryd, *Methods in membrane lipids*, 2015, pp. 91–102.
90 L. Szente and É. Fenyvesi, *Struct. Chem.*, 2017, **28**, 479–492.
91 M. Rahimi, D. Regan, M. Arroyo, A. B. Subramaniam, H. A. Stone and M. Staykova, *Biophys. J.*, 2016, **111**, 2651–2657.
92 E. London, *Acc. Chem. Res.*, 2019, **52**, 2382–2391.
93 Z. Huang and E. London, *Langmuir*, 2013, **29**, 14631–14638.
94 Q. Lin and E. London, *PLoS One*, 2014, **9**, e87903.
95 G. Li, J. Kim, Z. Huang, J. R. St. Clair, D. A. Brown and E. London, *Proc. Natl. Acad. Sci. U. S. A.*, 2016, **113**, 14025–14030.
96 G. Li, S. Kakuda, P. Suresh, D. Canals, S. Salamone and E. London, *PLoS One*, 2019, **14**, e0223572.
97 P. Suresh and E. London, *Biochim. Biophys. Acta, Biomembr.*, 2022, **1864**, 183774.
98 M. Varma, F. Khuri-Makdisi and M. Deserno, *J. Chem. Phys.*, 2024, **161**, 114103.
99 S. Foley and M. Deserno, *J. Chem. Theory Comput.*, 2020, **16**, 7195–7206.
100 I. R. Cooke, K. Kremer and M. Deserno, *Phys. Rev. E: Stat., Nonlinear, Soft Matter Phys.*, 2005, **72**, 011506.

101 I. R. Cooke and M. Deserno, *J. Chem. Phys.*, 2005, **123**, 224710.
102 M. Deserno, *Macromol. Rapid Commun.*, 2009, **30**, 752–771.
103 G. Orädd, P. W. Westerman and G. Lindblom, *Biophys. J.*, 2005, **89**, 315–320.
104 F. Weik, R. Weeber, K. Szuttor, K. Breitsprecher, J. de Graaf, M. Kuron, J. Landsgesell, H. Menke, D. Sean and C. Holm, *Eur. Phys. J.: Spec. Top.*, 2019, **227**, 1789–1816.
105 G. S. Grest and K. Kremer, *Phys. Rev. A: At., Mol., Opt. Phys.*, 1986, **33**, 3628.
106 A. Kolb and B. Dünweg, *J. Chem. Phys.*, 1999, **111**, 4453–4459.
107 M. Deserno, *Chem. Phys. Lipids*, 2015, **185**, 11–45.
108 M. P. Do Carmo, *Differential geometry of curves and surfaces: revised and updated*, Courier Dover Publications, 2nd edn, 2016.
109 A. J. Sodt, M. L. Sandar, K. Gawrisch, R. W. Pastor and E. Lyman, *J. Am. Chem. Soc.*, 2014, **136**, 725–732.
110 T. M. Konyakhina, S. L. Goh, J. Amazon, F. A. Heberle, J. Wu and G. W. Feigenson, *Biophys. J.*, 2011, **101**, L8–L10.
111 F. A. Heberle, R. S. Petruzielo, J. Pan, P. Drazba, N. Kucerka, R. F. Standaert, G. W. Feigenson and J. Katsaras, *J. Am. Chem. Soc.*, 2013, **135**, 6853–6859.
112 R. D. Usery, T. A. Enoki, S. P. Wickramasinghe, M. D. Weiner, W.-C. Tsai, M. B. Kim, S. Wang, T. L. Torng, D. G. Ackerman, F. A. Heberle, et al., *Biophys. J.*, 2017, **112**, 1431–1443.

Open Access Article. Published on 14 januar 2025. Downloaded on 30-01-2026 17:48:09.
This article is licensed under a Creative Commons Attribution 3.0 Unported Licence.